Accepted Manuscript

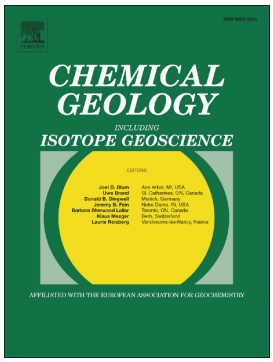

Vorontsovka Carlin-style gold deposit in the North Urals: Mineralogy, fluid inclusion and isotope data for genetic model

I.V. Vikentyev, E.E. Tyukova, O.V. Vikent'eva, A.V. Chugaev, E.O. Dubinina, V.Yu. Prokofiev, V.V. Murzin

PII: S0009-2541(18)30351-6
DOI: doi:10.1016/j.chemgeo.2018.07.020
Reference: CHEMGE 18848

To appear in: *Chemical Geology*

Received date: 19 December 2017
Revised date: 12 July 2018
Accepted date: 13 July 2018

Please cite this article as: I.V. Vikentyev, E.E. Tyukova, O.V. Vikent'eva, A.V. Chugaev, E.O. Dubinina, V.Yu. Prokofiev, V.V. Murzin , Vorontsovka Carlin-style gold deposit in the North Urals: Mineralogy, fluid inclusion and isotope data for genetic model. Chemge (2018), doi:10.1016/j.chemgeo.2018.07.020

VORONTSOVKA CARLIN-STYLE GOLD DEPOSIT IN THE NORTH URALS: MINERALOGY, FLUID INCLUSION AND ISOTOPE DATA FOR GENETIC MODEL

I.V. Vikentyev[1,2*], E.E. Tyukova[1,3], O.V. Vikent'eva[1], A.V. Chugaev[1], E.O. Dubinina[1], V.Yu. Prokofiev[1], V.V. Murzin[4]

[1] Institute of Geology of Ore Deposits, Russian Academy of Sciences (IGEM RAS), 35, Staromonetny per., 119017 Moscow, Russia

[2] Peoples' Friendship University of Russia (RUDN University), 6, Miklukho-Maklaya str., 117198 Moscow, Russia

[3] Scientific Geoinformation Center, 11, New Arbat str., Russian Academy of Sciences, 119019 Moscow, Russia

[4] Zavaritsky Institute of Geology and Geochemistry, Uralian Brunch, Russian Academy of Sciences (IGG UB RAS), 15, Akad. Vonsovskogo Str., 620016 Ekaterinburg, Russia

*Corresponding author: e-mail viken@igem.ru, phone +7-499-2308256

Submitted to Chemical Geology, December 2017

ABSTRACT

The Vorontsovka gold deposit in the Tagil zone, North Urals, hosts 101 t Au, averaging 7 g/t Au and including 30 t Au in the regolith, and 120 t Ag, averaging 8 g/t Ag. Early skarn-magnetite mineralisation related to a dioritic intrusion of the shoshonitic series was formed in the Late Emsian. Water and volatiles (mainly CO_2) released from host metapelites and limestones were mixed with the metalliferous magmatic fluid during catagenesis to contact metamorphism. The modified fluid extracted ore components from host rocks and syn-volcanic stratiform mineralisation and became enriched in Fe, Mn, Ba, Zn, Pb, Au, Ag and S to deposit these components as sulphide dissemination in the footwall of siliciclastic unit and underlying limestone both brecciated along the trust. At the final Early Eifelian stage, there was an additional inflow of deep mantle/magmatic fluid, enriched in Au, Hg, As, Sb and Tl. The mixing of this fluid with metamorphic water resulted in Carlin-style gold-realgar-stibnite (+Tl minerals) mineralisation mainly in carbonate breccia. The main gold endowment associates with gold-arsenic ores located in brecciated silicified limestone (jasperoid) and argillised tuff-siltstone. Early ore assemblages were formed at 510–240 °C (including magnetite skarn), whereas overprinting Carlin-style gold-(Fe, As, Sb, Hg, Tl) sulphide mineralisation was deposited at decreasing temperatures mainly from 260 to 110 °C. Fluid inclusion data revealed aqueous-carbonic, Ca-, Na-, Mg- and K-chloride compositions of ore-bearing fluid of 4.8-9.3 wt.% eq. NaCl. Changing fluid pressure corresponded to near lithostatic (0.5-0.6 kb) to hydrostatic (0.15-0.2 kb) conditions. Based on the $\delta^{34}S$ ranges of sulphides determined for siliciclastic rocks (–2.3 ... +1.8 ‰) and skarns (–2 ... +1.6 ‰) it is assumed that most of the sulphur derived from magmatic reservoir associated with the mantle. The lead isotopic compositions of sulphides show a relatively narrow range and continue the linear trend of the Early Silurian VMS deposits corresponding to the mixing line of mantle and crustal lead sources. Model Pb-Pb ages for the Vorontsovka sulphides are grouped into two clusters: 425-416 and 398-388 Ma. The second period is close to the U-Pb isotope age of the final stage of the Auerbakh pluton as well as in a good agreement with the Ar-Ar isotope age of 391.1 ± 4.9 Ma of hydromica from the late gold-arsenopyrite assemblage. The specific features of the Vorontsovka deposit indicative of the Carlin-style mineralisation are as follows: the paleo-continental margin and trust-related position; causing high-K/shoshonitic igneous activity; the fine-disseminated sulphide mineralisation in the highly brecciated carbonate-clastic sequence; jasperoid and argillic alteration accompanying gold orebodies with assay boundaries; multiple fluid source; Au-As-Hg-Tl geochemical association; the abundance of As- and As-Fe-sulphides and As-Sb sulphosalts; the occurrence of Hg-, Tl-sulphides and sulphosalts; the association of gold with arsenian pyrite and arsenopyrite overgrowing previously forming pyrite; and the predominance

of submicroscopic gold in the ores. A LA-ICP-MS analysis of pyrite confirms that elevated concentrations of Au regularly correlate with higher contents of As, Ag, Sb or Tl.

Key words: Vorontsovka gold deposit, Carlin-type, jasperoid, argillic alteration, mercury, arsenic, tallium minerals, sulphides, fluid inclusion, stable and lead isotopes

1. Introduction

The Turya-Auerbakh mineral district in the Krasnoturyinsk area, Ekaterinburg region, is situated to the Tagil zone restricted by the Main Uralian Fault in the west (Fig. 1). The mineral district, including the Vorontsovka Au deposit, covers the Turya-Auerbakh volcano-tectonic depression, occupying the southern part of the Early to Middle Devonian volcano-plutonic belt (Yazeva et al., 1989; Minina, 1994). According to paleotectonic reconstructions (Koroteev et al., 1997; Herrington et al., 2005; Puchkov, 2010; Yakubchuk, 2017), the Tagil zone incorporates fragments of an island arc, evolved mainly on ancient oceanic crust in the Late Ordovician to Late Silurian and then in the regime of the active continental margin (continental arc) in the Emsian to Eifelian epoch. Contrast volcanic basalt-rhyolite sequences were produced by island-arc volcanism that started in the Tagil zone at the end of the Ordovician (Tagil arc). Subduction-related regional tectonics was accompanied by local (backarc?) extension with the formation of large calderas, which hosted Cu-Zn volcanogenic massive sulphide (VMS) deposits (Vikentyev et al., 2017), commonly spatially related to felsic domes. This process intensely occurred in the Silurian (rhyolite-basalt and andesite-basalt series). In the Early Devonian (Emsian) subalkaline igneous series marked continental margin regime. Middle Palaeozoic subduction-related volcanism has terminated in the Middle Devonian (Eifelian) and during the Emsian-Eifelian period it was likely related to the formation of another (Magnitogorsk) arc, mainly in the South Urals (Puchkov, 2010).

The arc-related volcano-sedimentary and magmatic series comprise a variety of Cu, Zn, Fe, Ti, V, Au, Cr, PGE ore mineralisation. For the Turya-Auerbakh mineral district, copper±iron-skarn and gold (Vorontsovka) deposits are most important. High-temperature post-magmatic origin of Cu/Fe-skarn deposits is proved, but origin of the Vorontsovka deposit remains controversial (e.g., Murzin et al., 2017). The Vorontsovka deposit is usually referred to the Carlin type of gold mineralisation (e.g., Sazonov et al., 1998; cf., Berger, Theodore, 2005; Emsbo et al., 2006; Berger et al., 2014). Pb-Pb and sulphur isotopic systematics are an important clue to distinguish between mantle and crustal components in parental magma and fluid, which generated the mineralisation. Therefore, these isotopic systems are a main focus in the

interpretation of the genesis of the Vorontsovka deposit. Additional fluid inclusion and mineralogical study was also conducted for the interpretation of the nature of the ore-forming fluid. Description of the content of field and laboratory studies and analytical procedures can be found online in Appendix A. Samples and analytical methods.

1.1. Magmatism and geotectonics overview

In the North Urals, the Middle to Late Ordovician ophiolitic complex is covered by the Upper Ordovician to Llandoverian basalt-andesite-dacite(rhyolite) Shemur Formation, which hosts VMS deposits (Fig. 1). It is overlain by the Upper Silurian andesite-basalt suites. These calc-alkaline rocks are replaced upwards by subalkaline differentiated basalt-trachybasalt-trachyandesite-trachydacite and then by weakly differentiated trachybasalt-trachyandesite volcanics (Vikentyev, 1996; Bochkarev, Yazeva, 2000; Nosova et al., 2000). The later Pridoli – Lochkovian high-K Tura volcanic suite belongs to the shoshonitic series.

Later, Early – Late Wenlock granitoids (quartz diorite, granodiorite, plagiogranite, granosyenite) have accompanied the basalt and basaltic andesite and contain porphyry copper mineralisation. The Late Silurian to Early Devonian diorite, monzodiorite, and monzonite form final phases of a composite basalt-diorite-trachyte-monzonite volcano-plutonic suite, related to the mature arc. These Late Ordovician to Early Devonian volcanic arc complexes are believed to be of intra-oceanic origin (Yazeva, Bochkarev, 1996; Puchkov, 2009).

Some geochemical signatures of the Late Silurian to Early Devonian igneous rocks (high Zr/Hf, Nb/Ta, La/Sc, Y/Zr ratios and ASI, low Cr, Ni, Co, Sc contents) indicate that a less depleted mantle was involved in the melting, with limited influence of aqueous fluid on the mantle protolith (Sazonova et al., 1997). Crustal contamination of melts (causing high Th/Ta, K/Ti, Ba/Nb, Pb/Nb ratios) was recorded for the rocks of the Tura suite (Nosova et al., 2002; Narkisova, 2005). An inflow of fertile asthenosphere as a result of destruction of subducting slab can provide an additional source of heat to explain a relatively high degree of partial melting of the mantle, as it is assumed in the models (Humphreys, 1995; Shervais, 2001).

The limestone of the Frolov-Vasilyev Unit (Pragian to Early Emsian) indicates an amagmatic pause that corresponds to the accretion of the Tagil arc to the microcontinent, the orogen rise and its denudation. Later, the mature Tagil volcanic arc was substituted by the andesitic calc-alkaline magmatism (of the Magnitogorsk arc(?), cf., Puchkov et al., 2009, or mantle plume activity). The Krasnoturyinsk Formation (Emsian to Early Eifelian) comprises andesite and andesitic dacite of normal and high alkalinity and is overlain by trachybasaltic andesite tuff. The preserved thickness of Devonian volcanic series is approximately 4-5 km. The Pragian-Emsian limestone with Emsian andesite and tuffite are intersected by dyke swarms of

potassic basalt, trachybasaltic andesite, gabbro-diabase, hornblende, and biotite lamprophyre. The Emsian–Early Eifelian igneous rocks have geochemical features of the active continental-margin setting (Kuz'min, 1985; Yazeva et al., 1989).

Subalkaline plutonic rocks of the area are also multiphase. The Emsian Verkhnelobva and Emsian-Eifelian Auerbakh complexes combine a series of small, 0.5–40 sq. km stock-shaped massifs (Fershtater et al., 1984). These plutons are co-magmatic with the above mentioned effusive series, being similar in geological position, chemistry and mineralogy (Malakhov, Churilin, 1972; Grabezhev et al., 2014). The initial phase of the Auerbakh Complex is the Middle Emsian gabbro-diorite; the Late Emsian coarse-grained granodiorite and quartz monzonite are the main phase. Their formation was followed by intrusion of small high-K, orthoclase-porphyry granite stocks in the Early Eifelian. Diorite, quartz diorite and granodiorite are dominant among the intrusive and subvolcanic facies.

Regionally, the intrusive bodies correspond to the main volcanic phases. Dioritoids of the Verkhnelobva pluton and its equivalents are chemically most similar to the andesites of the Krasnoturyinsk Formation. Dioritoids of the Auerbakh Complex correspond to the subalkaline volcanic rocks, overlaying the Krasnoturyinsk Formation. All Devonian igneous rocks are represented by volcano-plutonic associations, in which intrusions are subject to or commensurate to the volume of the volcanic members. Overall, the postcollisional magmatism, first appearing in the Emsian, gradually spreads eastward, i.e., inward the active continental margin. Deformations of the Pragian-Eifelian rocks were associated with Early Carboniferous and Early Permian stages of collisional processes (cf. Vikentyev et al., 2017).

1.2. Geological setting

The Vorontsovka Au deposit (also spelled as *Vorontsovskoe*) is mainly located in carbonate rocks near the western contact of the Auerbakh gabbro-diorite-granodiorite pluton (Sazonov et al., 2001; Herrington et al., 2005). The pluton intrudes the large (35 x 18 km) Turya-Auerbakh volcano-tectonic graben-syncline (Fig. 2). The deposit is confined to the monoclinal limb of this structure, gently (20°-40°) dipping to the west. The limb is composed of andesitic volcano-sedimentary rocks of the Krasnoturyinsk Formation (Fig. 3), subdivided into three units. The lower *Frolov-Vasilyev Unit* (up to 1200 m thick) is composed of reef limestone with thin interbedded tuffaceous sandstone and siltstone. The limestone contains remnants of conodonts, brachiopods, and corals of the Emsian age.

In the upper contact zone, there is a brecciated limestone horizon with variable thickness (up to 100 m) hosting most gold orebodies. The breccia is represented by semi-rounded and angular limestone fragments, up to 25 cm, cemented by clay-carbonate and volcano-sedimentary

matrix: siliceous and calcareous-siliceous tuffaceous sandstone, siltstone and mudstone with pyroclastic fragments of plagioclase, amphibole and rarely pyroxene, and fragments of andesite, rarely andesitic dacite. The amount of cement in matrix breccias ranges from 20-30 to 60 vol% (Sazonov et al., 1991). Relics of layered texture often remain in the cement. Impregnation and thin layers of pyrite ± marcasite in the amount of 3-5 vol%, up to semi-massive sulphide lenses, occur in the breccia matrix. Locally in the areas of dyke swarm (upper horizons of the North pit), cement is represented by andesite lava or subvolcanic facies, and this rock can be described as an explosive agglomerate or xenoclastolava with abundant limestone fragments (Vikentyev et al., 2016b). Several models for formation of "limestone breccia" are considered including: (1) eruptive, (2) tectonic, (3) sedimentary, and (4) volcano-sedimentary.

The *first model* proposes that the eruptive breccia was formed by volcanic material filling the cavities in poorly cemented limestone under high fluid pressure during volcanic explosions (Sazonov et al., 1991). According to the model of *tectonic origin*, the breccia was formed due to the thrust-related movements coincident with the Auerbakh intrusion (Rakhov, 1999). According to the *sedimentary* and *volcano-sedimentary models*, the breccia, together with layers of tuffaceous sandstone and siltstone, was accumulated in syn-consedimentational depression on a submarine volcano slope due to destruction of the reef edifice (Minina, 1994; Cheremisin, Zlotnik-Khotkevich, 1997). It is impossible to exclude joint or multi-phase action of several mechanisms, as their corresponding characteristics are mapped in the Vorontsovka area.

Above are the unconformably overlying flysch-like volcano-sedimentary rocks of the *Bashmakov Unit* (120-450 m thick), represented by thin-interbedded fine-clastic andesitic tuffites (siliceous, calcareous), tuffaceous sandstones, andesite and basaltic andesite tuffs, and interlayers of ash-contaminated limestone. The overlying *Bogoslovsk Unit* (~200 m, up to 1000 m thick) occurs at the northern and southern flanks of the deposit. It is composed of crystalline-tuff, agglomerates of andesite and basaltic andesite, siliceous tuffaceous sandstone with lenses of limestone and andesitic lava flows.

On the contact with the Auerbakh pluton, the limestone is marmorised and widespread hornfels haloes occur. The Emsian-Lower Eifelian volcano-sedimentary sequence, hosting the gold orebodies, is cut by numerous diorite and mafic dykes. Some diorite dykes are skarn- and propylite-altered and accompanied by magnetite-sulphide mineralisation along contacts. Mainly NW-striking gabbroic and lamprophyric (kersantite, vogesite, spessartite) dykes are also widespread (Fig. 3).

1.3. Gold-bearing orebodies

The main lens-like orebodies are confined to a low angle thrust-disturbed contact of limestone in the footwall and thinly interbedded, siliciclastic sediment, in the hanging wall (Fig. 3, 4). The orebodies are controlled by the crushing zone that accompanies gently (45°-55°) west-dipping Vorontsovka trust (① on the Fig. 3). Flat (20°-40°) monoclinal western dipping of gold-bearing rocks (Frolov-Vasilyev and Bashmakov Units) is complicated by a large gentle anticline, the axis of which has a North-Western strike. The wavelength of the fold reaches 800-900 m, the limbs are complicated by a series of small (wavelength up to 80 m) anticlinal and synclinal folds.

Hydrothermal alterations comprise: early garnet-pyroxene and garnet-magnetite skarn; skarnoid (epidote-garnet and epidote skarn); later propylitic (chlorite-epidote-actinolite-albite) and beresite (quartz-sericite-carbonate-pyrite) alteration; and overprinting, gold-bearing phyllic (quartz-sericite), jasperoid and argillic alteration (Fig. 4). Argillic parageneses, containing kaolinite, dickite, illite-smectite, celadonite, are formed at the final low temperature stage. Mineralising zone is restricted by the steep (70°-80°) west-dipping Vorontsovka reverse fault (② on the Fig. 3) in the west. Supergene zone, karst and deluvial-proluvial and lacustrine-alluvial gold placers were formed in the Jurassic (Barannikov et al., 2016).

Initially, the Vorontsovka deposit contained 101 t Au, averaging 7 g/t Au, and 120 t Ag, averaging 8 g/t Ag; including 30 t Au in regolith (Bobrov, 2013). The deposit is mined by Polymetal Company from 1999 in two open pits to a depth of 200 m and 80 m. In 2009 Polymetal Company reported JORC-compliant reserves of 61 t Au and 82 t Ag; with additional mineral resources of 70 t Au and 100 t Ag. Orebodies correspond to the fine-disseminated low-sulphides (3-5 vol%, rarely up to 30 vol%) zones; gold-quartz veinlets occur rarely. The orebodies comprise 8 types of sulphide-disseminated ores (Fig. 5; see table 5), but the main gold endowment associates with the following two ore types: the gold-pyrite-arsenopyrite ore in the argillic altered tuff-clastic rocks (type 5/6) and the gold-pyrite-realgar ore in the silicified limestone breccia with relict carbonate-volcanoclastic cement (type 7).

2. Mineral assemblages

There are *four groups of mineral assemblages* in the orebodies of the Vorontsovka deposit (table S1). The later assemblages often overprint the early ones. *Group 1* comprises of pyrite ± sphalerite ± chalcopyrite ± pyrrhotite and is located in the limestone breccia and in the lowest part of the overlying tuff-clastic rocks. The carbonate breccia contains minor sub-layered fine-disseminated magnetite in its siltstone cement. The mineral assemblage, similar to the poor VMS ores, contains fine impregnation or linear aggregates of sulphides, mainly pyrite (Fig. 5a).

Microscopically, pyrite forms fine-grained euhedral zonal crystals and relicts of framboids (Fig. 6 a,b). According to the LA-ICP-MS study, the pyrite contains up to 1.5 wt% As (table 1).

Group 2 comprises fine-disseminated gold-pyrite-arsenopyrite in the tuff-clastic rocks. Such sulphide impregnation is locally redistributed with segregation into pyrite veinlets (Fig. 5b). Pyrite forms euhedral crystals and spherical aggregates (from 0.01 to 0.n mm). Arsenopyrite commonly occurs in the tuff-clastic rocks if they have evidences of hydrothermal alteration and primary pyrite recrystallisation. The As/S atomic ratio is close to 1 (Fig. 7a).

Group 3 includes garnet-magnetite prograde skarn; epidote retrograde skarn; brecciated carbonate rock with cocarde texture; polysulphide-carbonate-quartz and massive chalcopyrite veins (Fig. 5c,d). In the skarn, overprinting sulphide association of pyrite ± pyrrhotite ± chalcopyrite ± sphalerite ± galena is common, i.e. sulphides are epi-skarn. Later, along with silicification, arsenopyrite ± pyrrhotite ± sphalerite ± fahlore + Pb-Sb-sulphosalts + native gold were formed. During the final mineralisation phase, pyrite + barite, together with carbonate and hematite were crystallised.

Pyrite forms euhedral crystals and their aggregates (up to 10 cm). Typically, the central part of the pyrite crystals does not contain arsenic and is surrounded by the area with few percents of arsenic, and the outer zone is represented by arsenopyrite (Fig. 6c,d). Arsenopyrite forms euhedral crystals (up to 2-3mm) and their aggregates in intergrowths with pyrite. Arsenopyrite aggregates are often cemented by galena, tennantite-tetrahedrite and Pb-sulphosalts. The As/S ratio in the arsenopyrite is <1 (Fig. 7b). Pb-Sb(±Cu, Ag, Bi) sulphosalts (tables S1) are common and form a dispersed impregnation and needle aggregates up to 2 cm in silicified marble. Tennantite-tetrahedrite occurs in significant quantities only in massive chalcopyrite veins. Together with minor to trace Pb-sulphosalts, it cements brecciated pyrite and arsenopyrite and intergrowths with stibnite in the later breccia-like ores.

Table 1. Trace elements in pyrite of the Vorontsovka deposit according to LA-ICP-MS data.

Ore type	$n_{samp.}$/ $n_{anal.}$	min-max/geometric mean (ppm)								
		Co	As	Au	Ag	Se	Te	Sb	Pb	Tl
VMS-like, in limestone breccia with sulphide cement	2/5	0.031-1.4 0.14	1.16-1.57% 1.34%	5.58-13.2 8.3	0.047-1.04 0.214	274-529 352	5.4-117 16.55	1.01-4.8 2.25	0.18-4.79 1.48	0.003-0.17 0.023
Fine-disseminated gold-pyrite-arsenopyrite in volcano-sedimentary rock	8/36	0.54-3760 52	57-11240 2192	0.006-14.9 1.15	<0.001-18.3 0.47	0.37-107.6 8.28	0.9-76.5 6.97	0.009-350 8.05	0.015-3000 29.05	<0.002-23 0.34
Quartz-carbonate alteration	7/22	0.47-3720 22.7	5.63-6200 275	0.003-80 0.22	0.001-5.27 0.1	0.11-66.9 2.23	1.64-66.2 9.87	0.042-227 4.5	0.007-340 4.68	0.001-719 0.097
Epi-skarn	4/15	0.87-557 63.6	14.8-12710 797.5	0.003-25.7 0.42	<0.001-6.05 0.023	0.04-67.7 2.62	4.8-50.5 16.65	0.004-27.1 1.18	0.033-337 5.63	0.002-0.66 0.007
Gold-polymetallic	2/3	10.4-239 60.66	1310-4360 2495	2.09-3.4 2.7	5.47-62.2 16.75	16-262 41.54	1.8-49 8.64	17.1-157 74.34	430-79200* 3660	0.052-0.17 0.086
Jasperoid	1/4	83.9-149 118	858-1281 1067	0.81-3.39 1.52	2.7-5.5 3.6	4.64-5.69 5.08	7.36-22 14.47	24-36.4 31.64	22.7-59 36.19	0.33-1.53 0.58
Fine-disseminated gold-realgar	1/7	7.6-1400 279	470-9510 1653	0.015-2.8 0.59	0.001-10.76 0.36	2.74-92.8 21.5	7.7-49 14.2	0.03-350 11.5	0.008-909 17.9	<0.002-23 0.19

*with fine inclusion of Gn (?).

Group 4. The Carlin-style gold-pyrite-realgar assemblage is superimposed over different breccias. The sequence of the mineral deposition is as follows: pyrite + arsenopyrite → (silicification) → Pb-Sb-sulphosalts + sphalerite + chalcopyrite → (argillisation) → native arsenic + S-löllingite + native gold → thallium minerals + stibnite + realgar + orpiment + native gold (Fig. 5e,f). Pyrite occurs in the central part of arsenopyrite aggregates. Pyrite crystals are often cemented by stibnite and realgar. The amount of *arsenopyrite* in this group increases, and it commonly demonstrated rhombic or prismatic habit (Fig. 8a,b,e) and arsenic-rich composition (Fig. 7d) with Te and Tl as common impurities. Arsenopyrite is cemented and partially corroded by native arsenic, as well as by löllingite (Fig. 8e, 9b). Moreover, As-arsenopyrite grows orthogonally on the prismatic elongated relics of S-arsenopyrite that appears to be earlier arsenopyrite from the previous mineralisation stage (Fig. 8c-d). The gold concentration in arsenopyrite reaches 315 ppm (av. 5-6 ppm Au); Au content fluctuations correlate with the thallium variations.

Native arsenic is found in the ores locally in the form of massive dark gray nodules and veinlets, up to 2-3 cm, in argillisite assemblage and in the form of small scattered dark inclusions in the breccia, impregnated with late sulphides of arsenic (realgar and orpiment), where the impregnation of cinnabar also occurs. Native arsenic forms rosettes (pseudocrystals) with a pronounced cleavage. Locally these rosettes replace "felt" of needle-shaped crystals (~0.01 mm) of arsenopyrite and löllingite (Fig. 9b). Native arsenic cements and corrodes arsenopyrite (Fig. 9a) and contains disseminated native gold inclusions, commonly located near the arsenopyrite relics.

In the late assemblages, a wide range of *thallium phases* occurs: weissbergite $TlSbS_2$, christite $TlHgAsS_3$, dalnegroite $Tl_4Pb_2(As,Sb)_{20}S_{34}$, picotpaulite $TlFe_2S_3$, philrothite $TlAs_3S_5$, chabournéite $Tl_4Pb_2(Sb,As)_{20}S_{34}$, routhierite $Tl(Cu,Ag)(Hg,Zn)_2(As,Sb)_2S_6$, pierrotite $Tl_2(Sb,As)_{10}S_{16}$, boscardinite $TlPb_4(Sb_7As_2)_9S_{18}$, imhofite $Tl_{5.8}As_{15.4}S_{26}$, parapierrotite $TlSb_5S_8$, jentschite $TlPbAs_2SbS_6$, gillulyite $Tl_2(As,Sb)_8S_{13}$, vorontsovite $(Hg_5Cu)_{\Sigma 6}TlAs_4S_{12}$, ferrovorontsovite $(Fe_5Cu)_{\Sigma 6}TlAs_4S_{12}$, tsygankoite $Mn_8Tl_8Hg_2(Sb_{21}Pb_2Tl)S_{48}$ (table S1; Fig. 10a). All these phases form microscopic inclusions, often in As-sulphides, and intergrowths with Hg-sulphides (cinnabar HgS, metacinnabar HgS, and polhemusite (Zn,Hg)S), Hg-sulphosalts (aktashite $Cu_6Hg_3As_4S_{12}$ and laffittite $AgHgAsS_3$), and native gold.

Native gold grains are very small (commonly micron- and submicron-sized, rarely up to 200 μm) in all mineral assemblages. Locally it is found in the interstitial forms (Fig. 8b), plate-like and imperfect crystals (Fig. 8e, 9a, 12d).

3. Mineral chemistry

Chemistry of major sulphides was studied by EPMA and LA-ICP-MS analyses. For *pyrite*, the distribution of As, Co and Ni, commonly structure-bound, is the most important. In the early pyrite from tuff-sedimentary semi-massive sulphide cement of carbonate breccia, arsenic is

evenly distributed, and its content is up to 1.6 wt% (table 1; Fig. 11; Fig. S1). In the semi-massive VMS-like ore, gold has a high positive correlation with Co, Cu, Zn, Se, Te, Hg (0.8-0.9) and negative correlation with Ni, Ge, As, Sn (from –0.7 to –0.8) and with As (–0.5). Silver has high positive correlation with Sb, Tl, Pb (0.8-0.9) and negative correlation with Cd (–0.66). Pyrite contains 5.58-13.22 ppm Au; 0.05-1.04 ppm Ag; 0.003-0.2 ppm Tl; 1.01-4.8 ppm Sb; 1.1-1.5 wt% As; 0.03-1.4 ppm Co; 0-4.5 ppm Ni. Co and Ni contents in the early pyrite are commonly <1 ppm.

Pyrite of skarn is characterised by uneven distribution of admixtures (Fig. S2). The content of As varies between 0.1 and 1 wt% (LA-ICP-MS), locally it reaches 2.25 wt% (EPMA), the Co content reaches 0.4 wt%. The content of Ni commonly ranges first ppm (up to 433 ppm).

Pyrite from the gold-pyrite-realgar assemblage is characterised by zonal As distribution; its content is 0.04-0.25 wt% (Fig. S3). The Co content in the pyrite ranges from 59 to 192 ppm, whereas the content of Ni varies slightly (616-768 ppm). This pyrite has elevated contents of Se (1.2-267 ppm), Au (0.16-3.33 ppm), and Tl (0.23-5.8 ppm); admixtures of Ag (0.26-9.9 ppm), Sb (0.2-25.7 ppm), Pb (1.6-1010 ppm) and Bi (0-16.8 ppm) often positively correlate. Coincident peaks of the last four elements, apparently due to submicroscopic inclusions of Pb-Sb(As) sulphosalts of variable composition, are commonly present in the pyrite laser alalyses.

Gold in pyrite. Profile ablation by LA-ICP-MS method (cf. Vikentyev et al., 2016a) shows that high Au concentrations are typically correlated with higher contents of As, Ag, Sb or Tl (Fig. S1-3). The study of some grains of pyrite ("mapping" regime) shows irregular distribution of As, Sb, Ag and Tl, shown by their fine "spotty" pattern. This may indicate occurrence of micro- and nano-inclusions of Au-compounds (with Ag, Tl, Sb). Pyrite from the early assemblages is characterised by the highest Au content (up to 80 ppm), and pyrite of the latest pyrite-gold-realgar ore assemblage has minimum Au content (up to 2.8 ppm, geom. av. 0.36 ppm). Probable occurrence of submicroscopic gold (and Au-compounds) inclusions in host sulphides is indirectly confirmed by significantly higher Au concentrations, defined by the method of instrumental neutron activation analysis of ~50 mg monomineral samples of pyrite and arsenical pyrite of the Vorontsovka deposit (Vikentyev et al., 2016b): pyrite with 0.2-0.6 wt% As contains up to 1200 ppm Au and As-pyrite with 2.8-8.5 wt% As contains up to 2777 ppm Au.

Composition of *arsenopyrite* is characterised by a polymodal distribution of As/S ratio (Fig. 7) that may indicate different hydrothermal events (Kholmogorov, Yakovlev, 1977; Tyukova, Voroshin, 2007). The sequence of the arsenic mineral crystallisation is as follows: Asp → As(s) → Lö → AsS → As_2S_3 and suggests that the reduced alkaline As-bearing fluid was followed to the end of the process by more oxidised and significantly more acidic sulphurous solutions (Kolonin et al., 1988). Non-stoichiometric composition of löllingite, with confused-needle morphology of its aggregates, indicates its rapid non-equilibrium crystallisation.

Sulphosalts occur in different mineral assemblages located in carbonate rocks. They can be subdivided into two groups: predominantly antimony group (boulangerite, zinkenite, bournonite, jamesonite) and substantially arsenic group (geocronite, guettardite, twinnite, enargite). Antimony sulphosalts are common for the earlier and higher-temperature skarn formation, while a group of As-sulphosalts, crystallised during the later hydrothermal stages, contain thallium, mercury and manganese, and these elements also form proper minerals (table S1-3). Crystallisation of Sb-sulphosalts is followed by formation of stibnite and arsenic sulphides (realgar and orpiment). Tetrahedrite and tennantite often co-exist. In the latest thallium and mercury-containing assemblages (e.g., table S3), aktashite is found (table S2).

Sphalerite composition was also changed during the ore formation. Sphalerite of the earliest VMS-like assemblages has high Fe content (15.7 mol% FeS). Sphalerite of skarn contains 2.5-5 mol% FeS, and sphalerite of the late mineral assemblages contains less than 2 mol% FeS. Sphalerite co-existing with bernarlottiite, contains up to 7.67 wt% Hg, whereas sphalerite, intergrowing with routhierite, contains up to 21.41 wt% Hg and 3.44 wt% Mn (Fig. 10a; table S3). In the final stages of the hydrothermal process, mercury forms sulphides (cinnabar, metacinnabar) and telluride (coloradoite).

The native gold fineness (Fig. 12a) decreases from the early to the late generations, from 960 ‰ to about 700 ‰, but in the skarn, in some cases, low-fineness gold, containing from 3 to 11 wt% Hg, is present. Late high-fineness gold also contains up to 3 wt% Hg. Native gold is inhomogeneous within some grains (Fig. 12c).

4. Fluid inclusion study and TPX-reconstructions

The studied primary inclusions of 0.01 mm in size or less are located in the central parts of carbonate grains, and along growth zones of its crystals in gold-bearing jasperoid. Two types of fluid inclusions are distinguished. The first type dominates and essentially contains gas with liquid carbon dioxide, and the second is represented by one- or two-phase inclusions with a filling close to 100%. Cryometric studies of vapour inclusions of the first type showed that the gas phase contained N_2 and CH_4 admixtures, decreasing the melting point of CO_2 from −58 to−62 °C. The solutions of one- or two-phase inclusions indicate the $CaCl_2$-H_2O-salt system, as evidenced by their eutectic melting temperature (−49 °C). The fluid most likely contains KCl in addition to dominant NaCl, which is indirectly confirmed by sharp acceleration of ice melting at temperatures close to eutectics of KCl-NaCl-H_2O (−23.5 °C) and KCl-H_2O (−10.6 °C) water-salt systems (Naumov et al., 2002; cf. Borisenko, 1977). The total salt concentration in inclusion solutions, according to the melting point of ice at −4 to −6 °C, is 6.4–9.2 wt% NaCl eq. Fluid inclusion homogenisation temperature (T_{hom}) is 100–150 °C (Fig. 13).

Primary two-phase gas-liquid inclusions in calcite of limestone breccia homogenised into the liquid phase at 212-125 °C and contain an aqueous solution with a salt concentration from 4.8 to 9.3 wt% NaCl eq. Eutectic temperatures from –37 to –32 °C indicate NaCl and $MgCl_2$

domination in the solution of these inclusions (Fig. 13), the density of the fluid is 0.92-1.00 g/cm^3.

In addition, temperature, pressure, and sulphur fugacity (P, T, $f\,S_2$) during formation of the main ore types were estimated using bicarbonate and sulphur-isotope geothermobarometry, as well as mineral thermometry based on the element distribution between coexisting pyrite, pyrrhotite, and arsenopyrite (Sazonov et al., 1991; Vikentyev et al., 2016b; Murzin et al., 2017). Early ore assemblages were formed at 510–240 °C (including skarn with sulphides), whereas the late gold-(Fe, As, Hg) sulphide-quartz mineralisation was deposited at decreasing temperatures from 260 to 110°C (see table 5). The lower deposition temperature of the late gold-bearing assemblages are confirmed by a fluid inclusion study for calcite of the impregnated gold-polymetallic ore in jasperoid and the fine-disseminated gold-pyrite±realgar ore in the limestone breccia (Naumov et al., 2002; Vikentyev et al, 2016b).

5. Isotope study

5.1. Sulphur isotope composition of sulphides

Pyrite and arsenopyrite as well as minor sulphides (sphalerite, pyrrhotite, chalcopyrite, galena and stibnite) from different mineral assemblages of the Vorontsovka deposit were analysed (table 2). The $\delta^{34}S$ values of sulphides vary from –7.8 to +6.9‰ ($\delta^{34}S_{mean}$ = –0.4‰) (Fig. 14). The $\delta^{34}S$ value for most Vorontsovka ores and rocks is close to zero and varies from –2 to +0.1‰ in skarn zones, from –0.5 to +1.8‰ for pyrites from siliciclastic rock and from 0 to +1.6 ‰ in the gold-pyrite-apsenopyrite assemblage.

Table 2. Sulphur isotopic composition of sulphides of the Vorontsovka deposit and from igneous rocks of the Auerbakh Complex.

Sample	Mineral	δ^{34}S,‰ V-CDT	Rock/ore type	Mineral association
Vr 11-1	Py	6.1	dusty disseminated from VMS-like ore (ore type 1, pyritised tuff-sandstone)	Py
Vr 10-23b	Apy	0.6	limestone with calcite veinlet and related fine arsenopyrite impregnation	Apy (+minor sulphosalts)
Tuff-clastic rock (ore type 1/5)				
Vr 10-16	Py	–0.5	dusty disseminated in siltstone	Py
Vr 10-14b	Py	1.0	coarse-grained, from veinlet in siltstone	Py, Ccp, Sp, Po
Vr 10-11a	Py	0.2	fine-grained (<1mm) and tiny framboidal pyrite from pyritised carbonate-bearing siltstone	Py, Apy, Sp, Ccp, Chl, Cb
Vr 10-11b	Py	–0.2	coarse-grained (up to 3mm), from pyritised carbonate-bearing siltstone	
Vr 10-11c	Py	1.8	coarse-grained, from Q-Ccp-Chl veinlet in altered siltstone	Py, Sp, Apy, Ccp, Qz, Cb, Chl
Vr 10-11d	Sp	1.3		
Skarn and skarnoid (ore type 3)				
Vr 5-3b	Py	–1.7	skarn	Py
Vr 10-17	Py	–0.9	epidote skarn	
Vr 10-18a	Gn	–2	carbonate-sulphide vein in epidote skarn	Sp, Gn, Cal
Vr 10-18b	Sp	0.1		
Vr 10-19a	Apy	–1.0	dusty disseminated from skarnoid	Apy
Vr 5-3a	Apy	–0.4	skarn	
Polysulphide quartz veins and jasperoid (ore type 4)				
Vr 10-15	Py	2.7	coarse-grained, from silicified skarnoid with Qz-sulphide vein	Py, Ccp, Po, Sp, Gn, Au, Apy
Vr 10-9b	Py	3.4	coarse-grained, from silicified skarnoid of breccias-like structure	Py, Apy, Ccp, Po, Au
Vr 11-7b	Py	6.9	silicified skarnoid of brecciated structure	Py
Vr 8a-1	Py	4.6	silicified skarnoid	Py, Sp
Vr 8a-2	Sp	3.4		
Vr 8b-1	Py	3.9	polysulphide Qz-veins in silicified skarnoid	Py, Ccp, Po, Sp, Gn, Apy, Au
Vr 8b-2	Sp	4		
Vr 8b-3	Gn	3.2		
Fine-disseminated gold-pyrite-arsenopyrite ore (ore type 5)				
Vr 10-14a	Py	0.0	fine-grained, from clastic rock	Py, Ccp, Sp, Po
Vr 10-10	Py	1.4	black laminated siltstone	Py, Ccp, Sp, Gn, Po, Au
Vr 10-8	Apy	1.2	dusty disseminated from siltstone	Py, Apy, Au
Vr 10-19b	Apy	0.5		Py, Apy
Vr 10-13	Apy	0.6		Apy
Vr 10-12a	Apy	0.2	episiltstone alteration with “diffuse” arsenopyrite impregnation	Apy, Sp, Au
Vr 10-22	Py	1.6	episkarn	Py
Argillic alteration (ore type 6)				
Vr 1/2	Apy	–1.9	argillisite	Apy, Py
Vr 1/3	Apy	–3.5	argillisite	
Vr 1/1k	Py	–2.1	argillisite	Py
Vr 1/1s	Py	–2	argillisite	
Vr 1/4	Py	–1.8	argillisite	
Vr 2/1k	Py	–3	argillisite	
Vr 2/1s	Py	–3	argillisite	
Vr 1/5	Stb	–4.6	argillisite	Stb, Apy, Py
Limestone breccia (ore type 7)				
Vr 11-2	Py	–0.4	dusty disseminated, from limestone breccia with fine-grained Py-Qz cement	Py, Rl, Pb-Sb-sulphosalts, Au
201/86.5	Py	–4.2	fine-grained, from limestone breccia	Py, Rl
347/70.5	Py	–7.8		
Igneous rocks of Auerbakh Complex				
209/37.05	Py	–2.9	quartz diorite	
224/46	Py	–2.4	diorite	
326/52.1	Py	–0.9	andesite porphyrite	
282/27	Py	2.7	gabbro	
335/166	Py	–0.4	basaltic andesite porphyrite	
355/48	Py	–0.3	basalt porphyrite	

The symbols of the minerals are: Py - pyrite, Ccp - chalcopyrite, Po - pyrrhotite, Sp - sphalerite, Apy - arsenopyrite, Gn - galena, Stb - stibnite, Au - native gold, Rl - realgar, Qz - quartz, Cal - calcite, Chl - chlorite, Cb - carbonate.

The $\delta^{34}S$ values of sulphides from the jasperoid are positive (+2.7...+6.9 ‰) unlike those from sulphides of argillic alteration (–1.8...–4.6‰) and from dispersed pyrite in the cement of ore-bearing limestone breccia (–0.4...–7.8‰).

5.2. Oxygen, carbon and Sr isotope compositions of carbonates

Isotope composition of C and O in the Vorontsovka deposit (Sazonov et al., 1998; Murzin et al., 2010) characterises calcite from the host limestone and carbonates from different ore types (table 3). Calcite from carbonate strata has $\delta^{13}C$ =1.3-2.3‰, $\delta^{18}O$ = 17.9-23.6‰ (Fig. 15). The $^{87}Sr/^{86}Sr$ ratios for calcite from limestone are 0.7074-0.7079 (Fig. 16). During formation of the gold-bearing hydrothermal alteration and gold ores, carbonates were formed with consistently lighter isotope composition of carbon and oxygen in a sequence: ore-bearing limestone breccias → jasperoids → skarns → quartz veins. The lack of isotopic evidence of organic carbon participation in the mineral-forming processes corresponds to low contents of organic carbon in the host rocks and ores of the deposit (Rakhov, 1999; Murzin et al., 2017).

Table 3. Isotopic composition of C, O and Sr of carbonates from the Vorontsovka area.

Rock/ore type	Sample, hole/depth, m	$\delta^{18}O$, ‰ V-SMOW	$\delta^{13}C$, ‰ PDB	$(^{87}Sr/^{86}Sr)_{norm}$
Vorontsovka gold deposit				
Hosted limestone	670/390	21.2	1.9	
	666/343.7	21	1.6	0.707788±7
	751/176.5	21.5	1.4	
Recrystallised limestone	395/131	18.8	1.3	0.707355±9
	606/111.3	17.9	1.7	
	903/80	23.4	1.6	0.707930±6
Limestone breccia (barren)	280/77.3	19.8	2.3	
	280/77.4	18.8	1.8	
	281/83.7	22.5	0.6	
	281/83.8	22.8	1.6	
	281/85.5	23.5	1.5	0.707819±8
	281/85.6	23.6	1.7	
	670/224.2	23.1	1.4	
	670/269.7	16.9	1.8	
	670/269.8	16.8	1.7	
Hydrothermally altered limestone breccia (gold-bearing, ore type 7)	666/257.7	18	–1.2	
	666/257.7	17.3	–2.6	0.707139±11
	751/108	16.8	0.5	
	751/109	18.3	–0.1	
	748/63.5	19.3	1.9	
	748/63.6	17.4	–1.8	
	748/74	18.1	–0.3	0.707697±10
	748/75	17.3	–0.2	
	275/118.6	16.6	1.8	
	276/151.2	18.1	2.1	0.707416±8
	276/151.3	18.6	1.8	
	276/154	18.3	1.9	
	276/155	19.1	1.7	
	276/156	18.3	1.8	
	21/121	19.8	2.1	
	276/170.8	22.7	2.1	0.707885±6
Gold-bearing jasperoid (ore type 4)	737-2*	17.1	–1.8	
	737-3	20.7	1.2	
	332/284.5*	16.2	–0.7	
	332/286*	14.9	–4.3	0.704803±6
	287/53.5	16.8	–2.1	
Sulphidised skarn (ore type 3)	396/84	13.4	–2.4	
	334/128.6	12.8	–4	0.706369±7
	1001/95	12.2	–2.9	
Turya ore field, gold-bearing Cu (±Fe) skarn deposits				
Vadimo-Aleksandrovka Cu-skarn	654	10.5	–7	
Auerbakh ore field, gold-bearing Fe skarn deposits				
Vorontsovka Fe-skarn	540	9.5	–5.6	
North Peschanka Fe-skarn	962	10	–3.9	
	964	11.3	–3.5	
Auerbakh ore field, gold-bearing quartz-sulphide veins				
Peschanka Au deposit	546	9.6	–6.3	
	844	9.5	–6.2	
	Pe1-(2)*	12.3	–7.1	
	Pe1-(1)*	11	–5	

Notes: *dolomite, other samples – calcite.

5.3. Lead isotope study

Lead isotopic compositions of the main sulphide minerals of the Vorontsovka deposit (pyrite, arsenopyrite and galena, table 4) show a relatively narrow range between 17.99 and 18.11 for $^{206}Pb/^{204}Pb$, 15.57 to 15.59 for $^{207}Pb/^{204}Pb$, and 37.88 to 37.99 for $^{208}Pb/^{204}Pb$. In addition, for reference and discussion of possible Pb-sources, we used galena samples of two age groups of VMS Cu-Zn deposits in the Middle and North Urals (table S4-6; see Fig. 1): for the Tagil arc – from medium-sized Tarnyer and small Kaban deposits (Late Ordovician – Early Llandoverian, ~450-440 Ma), large San-Donato, small Valentor and Galka deposits (Llandoverian, ~440-435 Ma); and for the North Magnitogorsk arc – from large Safyanovka deposit (Eifelian, ~395-385 Ma).

Table 4. Pb-isotopic characteristics of minerals from the Voronitsovka deposit, North Urals.

Sample	Mineral	Description		$^{206}Pb/^{204}Pb$	$^{207}Pb/^{204}Pb$	$^{208}Pb/^{204}Pb$	T_M, Ma	μ_2	ω_2	Th/U
Vr10-11a	fine-grained pyrite (up to 0.05mm)	tuff-siltstone	sulphidised (up to 50 vol%)	18.0012	15.5734	37.8996	416	9.67	37.04	3.83
Vr10-11b	coarse-grained pyrite (up to 3mm)		sulphidised (up to 50 vol%)	17.9937	15.5749	37.8935	425	9.67	37.09	3.84
Vr10-14b	coarse-grained pyrite clusters up to 2cm		sulphidised (up to 20 vol%)	18.0185	15.5815	37.9386	420	9.7	37.29	3.84
Vr 8 g	galena	polysulphide veins	Qz-sulphide vein	17.9884	15.5725	37.8831	424	9.67	37.03	3.83
Vr10-18g	galena		Cb-sulphide vein in epidote skarn	18.0111	15.5805	37.9191	423	9.7	37.22	3.84
Vr 18	galena		Cb-Sp-Gl vein in epidote skarn	17.9867	15.5714	37.8791	423	9.66	36.99	3.83
Vr57-1	galena		Gl-Qz-Cb vein	18.0112	15.5824	37.9261	428	9.7	37.31	3.85
Vr75	galena		Gl-Qz-Cb vein	18.0291	15.5931	37.9746	435	9.75	37.65	3.86
Vr10-22	pyrite	fine-disseminated gold-pyrite-arsenopyrite ore	epi-skarn	18.0218	15.5715	37.8971	397	9.65	36.83	3.82
Vr10-14a	fine-grained pyrite (up to 0.05mm)		metaterrigenious	18.0262	15.5689	37.8968	388	9.64	36.73	3.81
Vr10-12a	arsenopyrite		metaterrigenious, with native gold	18.0332	15.5762	37.9121	398	9.67	36.92	3.82
Vr 10-13	arsenopyrite		metaterrigenious	18.0707	15.5857	37.9845	389	9.7	37.22	3.84
Vr10-19b	arsenopyrite		skarnoid	18.1060	15.5814	37.9913	353	9.67	36.89	3.82

6. Discussion

Comprehensive geological, mineralogical, fluid inclusion, stable and radiogenic isotope study showed that Vorontsovka represents complicated mineralising system with polygenic and polychronous features. It is an example of overprinting of Carlin-style mineralisation onto tectonically (mainly by trust) disturbed carbonate-clastic sequence previously locally altered into barren skarn and skarnoid. Early magnetite-garnet skarn related with the Late Emsian magmatism evolved to retrograde epidote skarn and propylite alteration with late sulphide deposition. Near (or immediately after) the Emsian/Eifelian boundary hydrothermal phyllic (quartz-sericite) and *Hg + As + Sb + fine-disseminated gold* sulphide mineralisation accompanied by jasperoid/argillic alteration were formed. It reveals complicated evolution of mineralising system, typical for many large Carlin-type deposits of Nevada (Teal, Branham, 1997; Norby, Orobona, 2002; Heitt et al., 2003; Cline et al., 2005; Meffre et al., 2016; Muntean et al., 2017 etc.). Mineralisation process at the Vorontsovka corresponded to general TPX-evolution trend with decreasing temperature, sulphur and oxygen fugacity.

Protolith, jasperoid/argillisite alteration, gold-hosting Hg-As-Sb sulphide mineralisation and trace-element geochemistry of the Vorontsovka deposit have obvious Carlin-signatures (for additional arguments, see sections 6.2 and 6.5). Moreover, both regions reveal temporal and spatial relation with shoshonitic (high potassic) magmatism (Berger, Bagby, 1991; Ressel, Henry, 2006; Ryskamp et al., 2008; Soloviev, 2014a), which is probably an important metallogenic prerequisite for the formation of large gold deposits in the continental margin environment (Muntean et al., 2011; Soloviev, 2014b; Hronsky et al., 2012; Johnson et al., 2015). Thus, regional and local geological features demonstrate affinity of Vorontsovka with Carlin-type deposits.

6.1. TPX-constrains of ore-genesis

New obtained data complement our early studies (Naumov et al., 2002; Vikentyev et al., 2016b; Murzin et al., 2017) and are consistent with previously received data showing the evolution of the TPX-parameters of gold-bearing fluid. The ores of the Vorontsovka deposit were formed from aqueous-carbonic, Ca-, Na-, Mg- and K-chloride fluids of 4.8-9.3 wt % eq. NaCl. Local co-existence of mostly liquid and mostly gaseous inclusions with equal homogenisation temperatures suggests a heterogeneous state of fluid as a result of boiling in shallow environment (Naumov et al., 2002). Fluid pressure fluctuates from near lithostatic (0.5-0.6 kb) to hydrostatic (0.15-0.2 kb) conditions during the tectonically active regime of volcano-plutonic arc, and the formation depth is estimated as ~1.5-2 km (Vikentyev et al., 2016b).

Our microthermometric data coincide with fluid inclusions data for Carlin-type, mainly in Nevada, and for Carlin-like, in China, Au deposits (Radtke et al., 1980; Cunningham et al., 1988; Lindblom, 1991; Groff et al., 2002; Zhong et al., 2002; Su et al., 2009; Gu et al., 2012), which were formed in a wide temperature (but mainly *low-temperature*) range from low to moderate

salinity fluids (Table S8). Vorontsovka fluids fall inside this field (Fig. 17). Temperature and salinity values of model fluids formed Carlin-type Au deposits are in the range of 150-200 ºC and of <6 wt % NaCl equiv., respectively (Hofstra, Cline, 2000). Further, Cline et al. (2005) have extended the interval of T_{hom} (~100 to 300 ºC) and salinity (0.5-8 wt %) of fluids (cf. Bodnar et al., 2014). Thus, the gold-bearing Vorontsovka fluids are very similar to the mineral-forming fluids of the Carlin-type deposits.

For skarn deposits in the Vorontsovka area, sulphide crystallisation begins in the pyrite stability field and later mineral assemblages form in the same field and the evolution trends commonly do not intersect the line of pyrite-pyrrhotite reaction as a temperature and $f\,S_2$ decrease. Slightly steeper trend (more rapid $f\,S_2$ drop relatively to temperature), cutting the line of pyrite-pyrrhotite reaction, is recorded for very distal skarn lenses on the Vorontsovka flanks. Sulphide deposition in the copper- and iron-skarn systems accompanied the temperature (from 600 °C to <200 °C), pressures (from 2-3 to 0.4 kbar), $f\,S_2$ (from 10^{-1} to 10^{-17}) and $f\,O_2$ decrease, while the alkalinity and tellurium fugacity increased (Murzin, Sazonov, 1999). Similar evolution trends are revealed for Vorontsovka (Fig. 18; table 5). Acidic solution migration through the crack system during phyllic and jasperoid/argillic alteration with sulphide mineralisation occured at the final stage of the ore deposition. Gold and sulphides were deposited at decreasing pressures (from 0.6 to 0.2 kbar) and temperatures (from 400 to 110°C) with gold fineness decrease from the early to late generations.

Table 5. Main ore types and TPX-conditions of ore mineralisation in the Vorontsovka gold deposit (adapted from Vikentyev et al., 2016b; Murzin et al., 2017).

№	Mineral ore type		Hydrotyhermal alteration			Ore mineral assemblages	Mega-stages*		*t*, °C	P, kbar	log *f* S_2
			Protolith	Type of syn-ore alteration							
1	VMS-like stratiform	fine-disseminated pyrite	siltstone, tuff-sandstone	hydrothermal-sedimentary silicification, sericitisation		(arsenopyrite) pyrite			350-250	0.1-0.2	–8…–12
2		fine-disseminated chalcopyrite-sphalerite-pyrite	carbonate breccia			chalcopyrite-sphalerite-pyrite			300-150 (100-10)**		–9…–14
3	Impregnated gold-magnetite-sulphide		marble, siltstone	hypogenous (hydrothermal)	skarn formation, propylitisation	bornite-chalcopyrite, pyrite-pyrrhotite-polymetallic	I	pre-'Carlin'	430-200	0.4-0.6	–5…–10
4	Impregnated gold-polymetallic				silicification, dolomitisation	arsenopyrite-pyrite, sulphosalts-polymetallic, sphalerite-arsenopyrite-pyrite, polymetallic			510-110	0.15-0.6	–7…–14
5	Fine-disseminated *gold-pyrite-arsenopyrite*		*siltstone, tuff-sandstone*, dykes		*silicification*, sericitisation	pyrite-arsenopyrite(As/S≤1)	II	Carlin-style	400-310	0.2-0.4	–7…–10
6	Gold-sulphide-argillic				*argillisation*	pyrite			200-120	0.15-0.2	–15…–18
7	Fine-disseminated *gold-pyrite-realgar*		*carbonate breccia*		*silicification* (jasperoid), decarbonation, phyllic alteration	pyrrhotite-arsenopyrite			370-300	0.2-0.4	–10…–12
						löllingite-arsenopyrite(As/S>1)			370-250	0.15-0.4	–12…–17
						pyrite-arsenic-realgar			260-110		–14…–17
8	Gold-oxide-clay		marble, siliciclastic rocks	*supergene oxidation*, leaching, hydration, hydrolysis		hydrohematite-jarosite			120-30	0.05-0.1	–15…–18

Notes:*see Fig. 18; **correspond to the sedimentation and diagenesis regimes. Major features are in italic.

6.2. Sources of fluid and ore metals

For skarn deposits, the sulphide crystallisation is the most low-temperature overprinting stage of the skarn alteration (Zharikov, 1970). Iron-skarn mineralisation in the Vorontsovka area was paragenetically associated with the gabbroic phase, and copper-sulphide mineralisation – with the later granitoid phase of the Auerbakh Complex (Baklaev, Usenko, 1989). According to the model of Poltavets (Dymkin, Koroteev, 1990), the main source of hydrothermal fluids for skarn-magnetite mineralisation is a deep magmatic chamber, in which the magmatic differentiation and separation of high-chlorine fluids and ore components occur repeatedly. Bulk geochemistry allows revealing sources of metals. Copper-skarn deposits contain a typical "mantle" set of elements: Fe, Cu, Co, Zn, Au, Te, S. For iron-skarn deposits with (mostly) the same specialisation, the role of tellurium drops considerably, while the role of lead rises, reflecting the increased contribution of the "crust" components in late mineral assemblages. At Vorontsovka, minerals of Fe, Zn, Cu, Pb are also common but As, Sb, Hg and Tl minerals are abundant. Native gold is Hg-rich, and minerals of Cu and Hg occur, i.e. there is a set of elements typical for the Au mineralisation related to the processes of differentiation of deep-seated, mantle-derived magmas. Therefore occurrence of Hg, Tl, Sb, As, Au and Cu minerals in the late assemblage may be signs of additional mantle-derived input into the hydrothermal system.

Sulphur isotope composition of sulphides from iron-skarn (Perkova, 1975; Baranov et al., 1985; Zagrudina, 1986) and copper-skarn (Perkova, 1975) deposits of the area suggests a high temperature deep-seated homogeneous source of sulphur, interpreted as a dominant mantle magmatic source.

Sulphur isotope composition of sulphides from *Vorontsovka* is mainly close to zero (Fig. 14; table 2): the $\delta^{34}S$ values for the siliciclastic rock are from –0.5 to +1.8‰, for the skarn are from –2 to +0.1‰ and for the gold-pyrite-apsenopyrite ores are from 0 to +1.6‰, showing the typical mantle values ($\delta^{34}S = 0 \pm 2$‰; Ripley, Li, 2003; Seal, 2006). 75% of all δ-values fall into a narrow interval from –3 to +3‰. It indicates that the predominant source of sulphur was mantle-related. In sulphides (pyrite, sphalerite, chalcopyrite) from jasperoid-related ores, the $\delta^{34}S$ value varies from +2.7 to +6.9‰. For pyrite from the VMS-like mineralisation in the volcano-sedimentary cement of limestone breccia, the $\delta^{34}S$ value is +6.1‰. Such positive values can be a result of the additional extraction of sulphur from the granodiorites (Murzin et al., 2017).

The $\delta^{34}S$ values of sulphides from the low-temperature argillisite are slightly negative (–4.6...–1.8 ‰). The disseminated pyrite from the ore-bearing limestone breccia cement (realgar assemblage, ore type 7) is also depleted by ^{34}S isotope ($\delta^{34}S$ = –7.8...–0.4 ‰). Deviation to negative $\delta^{34}S$ values probably indicates involvement of diagenetic sulphur, and the presence of the relict fine-globular and framboidal pyrite in the protolithic volcano-sedimentary rocks (Fig. 6a,b) supports this model.

Isotope analysis of carbonates reveals that the most isotopically light carbon, with value close to mantle, is typical for calcite from pyrite-chalcopyrite ore of the Vadimo-Aleksandrovka

copper-skarn deposit ($\delta^{13}C = -7.0‰$) and carbonates in quartz veins and veinlets with pyrite-polymetallic mineralisation. The most isotopically heavy carbon (and oxygen) is typical for limestone ($\delta^{13}C = 1–3‰$). Ore-stage Vorontsovka calcite and calcite from the iron-skarn deposits have the intermediate C-O values (Fig. 15).

Isotopic composition of the host limestone carbonate for Vorontsovka ($\delta^{13}C$=1.3–2.3‰, $\delta^{18}O$=17.9–23.6‰) corresponds to the Emsian marine carbonates (Veizer et al., 1999; Jaffrés et al., 2007). $^{87}Sr/^{86}Sr$ ratios of calcite from limestone (0.7074-0.7079; Fig. 16) are close to the average value of the Emsian marine carbonates (0.7081; Veizer et al., 1999). Carbonates of sulphide-rich jasperoid and magnetite-pyrite ore in the skarn have the lowest values of $^{87}Sr/^{86}Sr$ corresponding to igneous rock values (0.703±0.002; Faure, 1986; Veizer et al., 1999). The strontium isotope composition of carbonate forms a single evolutionary trend from the marine limestone to the mantle (Fig. 16). The presence of two main isotopic reservoirs of fluid: (1) fluid balanced with limestone ("metamorphic fluid"), and (2) mantle-related magmatic fluid were probable. Fluids from both were mixed in various proportions that is emphasised by the C-, O- and Sr-isotope correlation trends for carbonates.

Isotopic composition of hydrothermal fluid ($\delta^{13}C_{CO2}$ and $\delta^{18}O_{H2O}$) equilibrated with the carbonates and quartz at 150-400°C was calculated using the equilibrium fractionation factors (Ohmoto, Rye, 1979; Zheng, 1993, 1999) (table 6). In addition, $\delta^{13}C_{CO2}$ and $\delta^{18}O_{H2O}$ were determined directly in fluid extracted from inclusions in three samples of ore quartz. The data show that quartz-sericite alteration and gold-arsenic ore of type 7 were formed from fluid with the isotope composition of $\delta^{13}C_{CO2}$, close to that of marine limestone (from –0.8 to 1.7‰). Oxygen isotope composition of the water phase of the fluid ($\delta^{18}O_{H2O}$), responsible for deposition of early high-temperature mineral assemblages of the ore, ranges from 12.7 to 13.7‰, corresponding to a magmatic source ($\delta^{18}O_{H2O}$ from 6 to 14‰; Bowman, 1998). The late low-temperature assemblage in the ore type 7 was formed from fluid with the $\delta^{18}O_{H2O}$ values varying from 7.1 to 9.6‰.

The calculated $\delta^{13}C_{CO2}$ values for the fluid equilibrated with minerals of the jasperoid (ore type 4) vary from –3.8 to –0.2‰. These values are lower than the values of the ore type 7 (see above) and coincide with the mantle carbon composition (–4 to –6‰; Faure, 1986). The direct measured $\delta^{13}C_{CO2}$ values from fluid inclusions ($\delta^{13}C_{CO2}$ = –3.2 to –2.8‰) are close to the calculated ones. The calculated oxygen isotopic composition of fluid ($\delta^{18}O_{H2O}$ = from 7.2 to 9.4‰) corresponds to magmatic water range (Hoefs, 1997; Bowman, 1998).

Table 6. H_2O and CO_2 isotopic compositions of fluid inclusions from quartz and calculation of isotopic composition of fluids that formed Vorontsovka gold deposit

Rock, host mineral (number of analysed samples)	Measured isotopic composition of minerals, ‰			$T_{av.}$, °C	Calculated isotopic composition of the fluid, ‰	
	δD, VSMOW	$\delta^{13}C$, PDB	$\delta^{18}O$, VSMOW		$\delta^{13}C_{CO2}$	$\delta^{18}O_{H2O}$
Ore breccia without realgar, calcite (4)	-	–2.6 to –0.1	17.3 to 18.3	350	–0.2 to 2.3	12.7 to 13.7
Ore breccia with realgar, calcite (6)	-	1.7 to 2.1	16.6 to 19.1	200	2.1 to 2.5	7.1 to 9.6
Jasperoid, dolomite (4)	-	–4.3 to –0.7	14.9 to 17.1	250	–3.8 to –0.2	7.2 to 9.4
Jasperoid, quartz (3)	-		13.9 to 15.6	250		4.5 to 6.2
Jasperoid, CO_2 from fluid inclusions in the quartz (3)	-				–3.2 to –2.8	
Jasperoid, H_2O from fluid inclusions in the quartz (3)	–74 to –53					
Fe-Cu skarns, calcite (7)	-	–7.0 to –2.4	9.5 to 13.4	300	–5.2 to –0.6	3.9 to 7.8
Quartz veins, dolomite (4)	-	–7.1 to –5.0	9.5 to 12.3	250	–6.6 to –4.5	1.8 to 4.6

Notes: To calculate $\delta^{13}C_{CO2}$ in carbonate, we used isotopic equilibrium calcite-CO_2 and dolomite-CO_2 (Ohmoto, Rye, 1979).
To calculate the $\delta^{18}O_{H2O}$, we used isotopic equilibrium calcite/water, dolomite/water (Zheng, 1999) and quartz/water (Zheng, 1993).

Fluids forming the skarn ore type 3 were ^{13}C- and ^{18}O-enriched ($\delta^{13}C_{CO2}$ from –5.2 to –0.6‰, and $\delta^{18}O$ from 3.9 to 7.8‰). The $\delta^{13}C_{CO2}$ values vary from –6.6 to –4.5‰ and $\delta^{18}O_{H2O}$ from 1.8 to 4.6‰ for late quartz veins in the exocontact of the Auerbakh pluton (table 6). These data confirm a possibility of partial isotope exchange between post-magmatic fluids and limestone. Skarn-forming fluid was separated from this chamber and interacted with the host rocks with sulphide mineral precipitation after magnetite skarn – with decreasing temperature. The ^{16}O-enrichment of fluids could be also affected by heated meteoric water input.

It is likely that hydrothermal solutions that formed Vorontsovka Au mineralisation were primary separated from the same diorite-granodiorite magma. Mineralising fluid was modified by its interaction with host rocks and addition of deep mantle-derived fluid and diluted metamorphic/meteoric water. Low-sulphide gold mineralisation was deposited at lower temperatures on the periphery of the skarn zones in shallow environment.

The presence of Hg-rich native gold (up to 5-11 wt %) (Vikentyev et al., 2016b; Murzin et al., 2017) suggests that sulphide mineralisation of the skarnoid and gold orebodies was linked to basaltoid magmatism (with possible fluid contribution from the mantle) (Murzin et al., 1981).

Our data on sources of Vorontsovka hydrothermal fluid do not contradict the data obtained for the Carlin-type deposits of Nevada (cf. Hofstra, Cline, 2000; Cline et al., 2005). Quadrupole mass-spectrometer gas data for quartz from the Goldstrike property, Turquoise Ridge deposit, and "metamorphic" quartz of the Getchell trend plot near the N_2 apex of N_2–Ar–He diagrams, which is indicative of a *magmatic* fluid end member (Groff, 2018). Carlin-type quartz contains liquid-dominant vapour-poor inclusions and is characterised by total gas contents >10 mol% and N_2/Ar values >300 that is consistent with *mixed crustal–meteoric–magmatic fluid sources*.

Fluid inclusions in quartz from veinlets and breccias interpreted as fluid pathways of the ore-forming fluid from the Carlin-type Gold Quarry and Chukar Footwall deposits have intermediate to low vapour/liquid ratios and salinities mostly between 1 and 7 wt % NaCl equiv.; they homogenise between 120 and 235 °C (Large et al., 2016). These data agree with previous values reported for ore-stage fluid inclusions in ore jasperoid Carlin-type quartz (T_h of 180–240 °C and salinities between 2 and 3 wt % NaCl equiv.; Cline, Hofstra, 2000; Cline et al., 2005). Fluid inclusions analysed by LA-ICP-MS are hosted in quartz intergrown with Au-bearing arsenian pyrite (Large et al., 2016). Comparison of the ratios of Rb, K, B, As, Sr, and Ba in fluid inclusions between clearly magmatic–hydrothermal Cu-Au ores at Copper Canyon porphyry deposit in the Battle Mountain–Eureka trend with the Carlin-type Gold Quarry and Chukar Footwall deposits on the Carlin trend reveals that both ore districts can be related to *upper crustal hydrous magmatic intrusions* and formed at different distances from their magmatic fluid source. Fluid compositions are best explained by separation of a *deep magmatic fluid* into Rb-K–enriched brine and B-As-Au–enriched vapour, followed by cooling and contraction of the magmatic vapour phase to an epithermal liquid, which reacted with Sr-Ba–bearing sedimentary rocks during ascent and eventual precipitation of Au-rich arsenian pyrite (Large et al., 2016).

6.3. Lead isotope systematics of sulphide mineralisation

Lead isotopic compositions of Vorontsovka sulphides, relative to the evolutionary curves and Stacey–Kramers isochrones, are shown on Fig. 18. Additionally, lead isotopic compositions of the VMS-hosted galena for the Tagil and North Magnitogorsk zones are also shown on the diagram. As for the VMS ores, the lead isotopic composition of galena for a single VMS deposit is homogeneous (Fig. 18; table S4). On a $^{206}Pb/^{204}Pb$–$^{207}Pb/^{204}Pb$ diagram, the isotopic domains of the VMS-hosted lead correspond to several fields and are clustered along a steep trend, cross-cutting the curves of lead evolution in mantle and orogenic geochemical reservoirs at a steep angle (Fig. 19; cf. Chernyshev et al., 2008). The lower part of the trend lies in the Pb-isotopic field, corresponding to a depleted mantle source of the DMM-A type. The points with model Pb-Pb age (Тм) 400 Ma form the upper part of the trend and lie between orogenic curve and the mean evolutionary curve of the Stacey–Kramers model (μ_2 = 9.74). Pb-isotopic composition field of ore minerals from the Vorontsovka deposit lies near data points of the Devonian Safyanovka VMS deposit. The latter deposits could have a uniform ore Pb source, which, by its geochemical parameters, is close to crustal sources. According to Pb-Pb data for Vorontsovka, the geochemical parameters of this source show that the evolution of lead before its separation as a result of the ore-forming process took place in the U–Th–Pb system with μ_2 ~9.68, ω_2 ~ 37.1, and Th/U ~3.83.

Average Pb-Pb model age calculated for all samples is 410 ± 23 Ma (±SD) which is close to geological age of the Vorontsovka host rocks (~408-390 Ma, table 4) and close to that of the Safyanovka and Sibai VMS deposits of the Magnitogorsk arc (~395-385 Ma, table S4). The model Pb–Pb age for the VMS deposits of the Tagil arc varies from 420 to 509 Ma (table S7), while μ_2 varies from 9.27 to 9.54. The Pb–Pb model age for the studied VMS deposits of the Magnitogorsk arc is ~420 Ma for Sibai and ~380 Ma at Safyanovka (close to their geological age of 395-385 Ma, table S7), while μ_2 slightly varies from 9.66 to 9.68. Taking into account some lead isotopic affinity of the VMS deposits, on the one hand, and the Vorontsovka deposit, on the other hand, we can conclude a similarity in geochemical characteristics of the sources, which contributed to the formation of these deposits.

A difference of the Pb isotopic composition in separate deposits is related primarily to the isotope-geochemical features of sources involved in their formation (Chernyshev et al., 2008). As to Vorontsovka, several sources may have been involved including: (1) buried Late Ordovician to Early Silurian VMS mineralisation; (2) VMS-like sulphide mineralisation disseminated in the host Late Silurian to Early Devonian volcano-sedimentary siliciclastic rocks; (3) water-rich volatile fluid derived from magma; and (4) a fluid derived from a deep-seated (possibly mantle-related) source, transported, for example, by trans-magmatic fluid flow (cf. Korzhinskiy et al., 1984; Luo et al., 2007).

6.4. Age of mineralisation and its relation to arc-related magmatism

Currently, several dates for volcano-plutonic rocks of the Auerbakh Complex indicate their formation in the Early Devonian, synchronously with the Krasnoturyinsk volcanic sequence. Krasnobaev et al. (2007) estimated 404.8±5 Ma U-Pb age of zircon (ion microprobe SHRIMPII) from quartz diorite of the Auerbakh pluton and 393 ± 3.3 Ma from granodiorite. Rb-Sr dating of the whole complex of igneous rocks (gabbro, gabbro-diorite, quartz diorite, granite) revealed the age 404.5 ± 9.1 Ma, which coincides with the U–Pb isotopic age of the zircons from the quartz diorite. Sm-Nd age (ID-TIMS) of the biotite-pyroxene-amphibole diorite is 411 ± 25 Ma (Ronkin et al., 2009). A concordant U–Pb age of zircon (16 crystals) from quartz diorite in the Turya ore field is 407.7 ± 1.6 Ma, that corresponds to the Early Devonian (Emsian) formation age of the copper-skarn systems at the Turya ore field (Grabezhev et al., 2014).

The age of the gold-arsenic mineralisation of Vorontsovka is debated. Some geologists attribute this mineralisation to intrusive magmatism, suggesting that the deposit is epithermal and distal skarn or copper porphyry (Minina, 1994). Porphyrytic diorite of the endocontact of the Auerbakh pluton hosts gold-bearing quartz veins and disseminated pyrite-chalcopyrite mineralisation with elevated Au and Ag concentrations. Skarn-porphyry copper deposits, similar to the Turya field deposits, are known in the south-western USA, spatially and temporally close to Carlin-type Au deposits (Einaudi et al., 1981).

It was proposed that Au mineralisation was related to tectonic events at the Carboniferous/Permian, Paleozoic/Mesozoic and even Mesozoic/Cenozoic boundaries, which might be responsible for the development of argillic and jasperoid alteration (Bobrov, 1991; Sazonov et al., 1991; Begetnev, 1999; Barannikov, Ugryumov, 2003).

New Ar-Ar data (Fig. S5) for the sample of hydromica 2M1 + 1M, extracted from a mica-carbonate vein that cuts limestone and gold-bearing tuffaceous siltstones with disseminated pyrite (an ore type 5), revealed 391.1±4.9 Ma, closely matching the age of the late igneous phases of the Auerbakh complex (393 ± 3.3 Ma, Krasnobaev et al., 2007). This Ar-Ar dating records a final stage in formation of gold-arsenic ores. Therefore, the Vorontsovka gold-arsenic ores formation was synchronous with granodiorite intrusion, finishing the magmatism of the Auerbakh Complex, or immediately followed it (Fig. S6).

Pb-Pb model ages for sulphides of the Vorontsovka deposit can be roughly grouped into two clusters: 425-416 and 398-388 Ma. The former cluster is close to the Sm-Nd isotope age of the earlier intrusive phases of the Auerbakh complex with age 411±25 Ma (Ronkin et al., 2009). The latter period corresponds to the Emsian-Eifelian age of the hosting volcano-sedimentary units (408-389 Ma), as well as to the U-Pb age for quartz diorite and granodiorite of the Auerbakh Complex (409-393 Ma), and coincides with the 391.1 ± 4.9 Ma Ar-Ar age of hydromica from the gold-arsenopyrite assemblage.

It is important to emphasize that for the Vorontsovka deposit possible VMS mineralisation occurs in the deep-seated Lower Silurian basalt-rhyolite sequences. Therefore, the sulphide

source for the Vorontsovka deposit may be partly related to such VMS bodies; correspondingly, the VMS mineralisation may have affected Pb-Pb characteristics of the Vorontsovka sulphides. At the same time, lead of the Vorontsovka gold-bearing sulphide assemblages reveals homogenic isotopic composition (Fig. 19, table 4), with a narrower Pb-Pb model age range (425-389 Ma). This may indicate that a single underlying fluid source – subvolcanic magmatic chamber related to andesitic arc – was predominant; this is consistent with the data on the sulphur isotopic composition of sulphides. Isotopic composition of C and O in calcite also indicates a significant contribution from a magmatic source (cf. Murzin et al., 2017).

6.5. Genetic model

It is proposed that Vorontsovka gold mineralisation was formed within the peripheral zone of porphyry copper system (Minina, 1994; Grabezhev et al., 2014). Naumov et al. (2002) also included this deposit into plutonogenic-hydrothermal clan. Our three-stage Vorontsovka formation model includes mixed post-magmatic, deep mantle-derived and metamorphic/meteoric fluid sources and improves the model proposed by Sazonov et al. (1991, 1998). Accumulation of disseminated sulphides and Fe-oxides-hydroxides and formation of stratiform pyrite mineralisation, similar to the poor VMS ore occurred during the first, syn-volcanic stage (Early-Middle Emsian). In shallow subvolcanic environment, post-volcanic fluids mixed with the buried sea waters and could result in local ore redistribution and its collective recrystallisation, leading to the formation of sulphide concretions and lenticular pyrite accumulations.

At the second stage (Late Emsian), intrusion of the shoshonite series pluton and accompanying dykes caused skarn alteration with formation of lenses and bands of skarn and magnetite ore at the contacts of silicate and carbonate rocks in the area. Waters derived by heating of limestone were mixed with metalliferous (Fe, Cu, Au and S) magmatic fluid and catagenic waters released during sediment compaction and lithification. Intrusion of large Auerbakh pluton was accompanied by local trusting. Heated and relatively aggressive waters extracted petrogenic and ore components, including some additional gold, from volcano-sedimentary rocks and syn-volcanic stratiform sulphide and Fe-oxide-hydroxide VMS-like mineralisation. The resulting fluid, enriched in S, Se, Te, Fe, Mn, Ba, Zn, Pb, Bi, Au and Ag, moved further to the surface. The steeply-dipping Vorontsovka fault on the western boundary of the structure (Fig. 3) limited further flow of hydrothermal solutions to the west. Trust-disturbed, brecciated footwall of siliciclastic unit and more permeable breccia bodies in the underlying limestone are favourable for disseminated sulphide deposition. The contact of limestone with overlaying thin bedded pyrite-bearing volcanic-siliciclastic rocks was a geochemical and petrophysical barrier (Fig. 20). Gold-sulphide and sulphide-polymetallic assemblages were also superimposed on the locally occurring barren skarn and skarnoid.

During the third, Carlin-style, stage (Early Eifelian), there was an additional input of deep mantle/magmatic fluids, enriched in Au, Hg, As, Sb and Tl. The mixing of this fluid with

metamorphic waters resulted in crystallisation of gold-realgar-orpiment-stibnite (+Tl-minerals) in carbonate rocks and pyrite+arsenopyrite in siliciclastic rock (Fig. 20). Mercury sulphides (cinnabar, metacinnabar) and telluride (coloradoite) were formed and Hg was incorporated in sphalerite and native gold. This stage is similar to ore style of the Carlin-type deposits (e.g., Radtke, 1985; Hofstra, Cline, 2000; Cline et al., 2005).

Position of the Vorontsovka Au deposit is a distal, peripheral zone of Fe-skarn deposit, but commonly they not substitute each other (see Fig. 2, 3) occurring at some distance. Locally, along some dyke contacts, Carlin-style mineralisation post-dates the sulphide mineralisation, which in turn, overprints narrow distal zone of magnetite skarn and epidote skarn.

Our model suggests significant role of magmatic source of fluids and metals in ore-genesis (cf. Sillitoe, Bonham, 1990; Kesler et al., 2005; Emsbo et al., 2006; Muntean et al., 2011; Large et al., 2016; Groff, 2018). A possible distal magmatic fluid source at the Carlin trend deposits is manifested by minor but widespread dykes of the same Eocene age (Ressel, Henry, 2006) clustering into several large igneous areas along the Carlin trend and correlates with the spatial position of Yellowstone hotspot in the Eocene (Oppliger et al., 1997; Hofstra, Cline, 2000). Comparative fluid inclusion study reveals that both ortho-magmatic porphyry and Carlin-type deposits can be related to upper crustal granitoid plutons but formed at different distances from the magma chamber (Large et al., 2016; cf. Sillitoe, Bonham, 1990). Fluid compositions evolved by brine/vapour separation of a deep magmatic fluid, followed by cooling and condensing of the magmatic vapour phase into an epithermal hydrothermal solution, which interacted with sedimentary host rocks and caused Au-rich arsenian pyrite precipitation demonstrating a model very close to Vorontsovka.

Major metallogenic characteristics of the Vorontsovka deposit were summarised in table 7 and table S9 containing compilation of similar features of most/some Carlin-type deposits.

7. Conclusions

The complex research, including mineralogical, fluid inclusion, stable and radiogenic isotope study, suggests multiple sources of fluids and metals in the Vorontsovka hydrothermal system. Mineralising fluid originated by interaction of the metal-bearing (Cu, Se, Te, Bi, As, Sb) magmatic fluid with host rocks and addition of deep mantle-derived fluid carrying Hg, Tl, Au, Cu, Co, Ni and diluted metamorphic/meteoric water. This fluid, carrying sulphur with $\delta^{34}S = 1 \pm 3$ ‰, formed Au-bearing sulphide mineralisation overprinting skarn as well as silicified limestone breccia (jasperoid) and argillic-altered siltstone/tuff-sandstone. During the ore deposition, carbonate was enriched in ^{12}C and ^{16}O isotopes in the following sequence: Au-bearing limestone breccia → jasperoid → skarn → quartz veins. The Sr isotopic composition of carbonate also forms a similar trend from a marine limestone to the mantle.

Table 7. Major features of Vorontsovka and Carlin-type deposits and their comparison.

Ore control factors	Features		Vorontsovka	Carlin-type deposits, adopted from Radke, 1985; Hofstra et al., 1999; Bettles, 2002; Cline et al., 2005; Ressel, Henry, 2006; Muntean et al., 2011*
Litho-stratigraphic	dominant host stratigraphic level		Lower Devonian	Silurian-Devonian
	host rock		breccia-like limestone and calcareous, fine-grained siliciclastic rocks, minor volcanics	silty carbonate rock and calcareous, fine-grained clastic rocks, in some cases (Vista Vein shear zone etc.) volcanic (Barber, 2015)
	lithological control		favourable horizons: reactive and permeable carbonate breccia under impermeable seal of finely laminated siltstones; carbonate-, pyrite-bearing siltstones and silty limestone	breccia-like and carbonaceous, silty carbonates and carbonaceous/ carbonate-bearing finely laminated siltstones and shales; shale-limestone contact: reactive and permeable limestone under impermeable seal of shales
	preore breccias		abundant: sedimentary breccia, hydrothermal-explosive breccias, locally tectonic breccia, xenoclastic lava breccia	commonly abundant: debris flow, hydrothermal dissolution collapse breccia, locally tectonic breccia, karst breccia
	carbonaceous matter		carbonaceous matter is present in the unoxidised ore (Murzin et al., 2017)	carbonaceous matter in some form is present in the unoxidised ore of most Carlin-type deposits; its abundance within orebodies is highly variable
Magmatic	moderately acidic plutonism		multiphase (Ordovisian – Eifelian)	multiphase (Jurassic, Cretaceous, Eocene, and Miocene); Eocene igneous episode was the largest and longest
	causative global process		deep mantle flow (plum), shoshonite and high-K calc-alkaline magmatism; anomalously active magmatism; signature of mantle components	deep mantle flow (plum), shoshonite and high-K calc-alkaline magmatism; anomalously active magmatism; signature of mantle components (Ryskamp et al., 2008; Johnson et al., 2015)
	metallogenic age		Mid-Paleozoic, Late Emsian-Early Eifelian ~405-391 Ma	Cenozoic, Eocene (~42-34 Ma)
	synchronous magmatic series		felsic and intermediate (dioritic to granitic, rarer gabbroic and lamprophyric) intrusive rocks, including sub-alkaline high-K ones, in the form of dykes, lavas and stocks	felsic and intermediate (dioritic to granitic, rarer gabbroic and lamprophyric) rocks, including sub-alkaline and shoshonitic, commonly in the form of dykes, lavas, and epizonal intrusions
	volcanism/plunonism		both very high intensity	both very high intensity
	main intrusion phase		granodiorite, monzodiorite	diorite, monzodiorite
	common dyke series		diorite, gabbro, monzonite, lamprophyre; most pre- and synore (altered); rarely postore (mafic)	rhyolite to dacite, rarer basaltic andesite, basalt and lamprophyre; syn- or immediately preore; rarely postore
Tectonic	regional	global	continental margin Mid-Paleozoic tectonics (rifted western margin of Kazakh? craton); slab-window-relation is probable	overthrust terranes related to continental margin tectonics (rifted western margin of North American craton); far back-arc position; slab-window-relation
		deep	renewed NS deep faults; ore deposits of different types occur aligned along NW hidden structures (Fig. 2); renewed NW deep faults are probable	renewed deep faults; ore deposits of different types and ages occur aligned along these basement structures of oblique mainly NW (at smaller extent NE) direction
		shallow	within a medium-scale thrust	within or adjacent to the Roberts Mountains and other regional thrusts
	trust-relation		main fluid-distribution structure hosting orebodies	regional fluid-distribution structure (aquitard); in some case it is ore-hosting
	local		both discordant (high-angle) and sub-comfortable (low-angle) faults, both with moderate to small displacement; thrust duplex (see cross-sections on Fig. 3); elongate large gentle anticline with NW plunge direction	both discordant (high-angle with moderate to small displacement) and sub-comfortable (low-angle thrusts and shears) faults; thrust duplexes with NNW elongate anticlinal zones

*additional to mentioned refs are given in parentheses.

Table 7 (cont.)

Alteration (unoxidised zones)	preore		skarn, peripheral propylitic, quartz-sericite	skarn, peripheral propylitic, quartz-sericite
	synore		decarbonation, silicification, argillisation, sulfidation	decarbonation, silicification, argillisation, sulfidation
	common synore minerals		illite-smectite, kaolinite, montmorillonite, dickite, celadonite	kaolinite, smectite, illite, illite-smectite, dickite
Geo-chemical	deposit series		Au-Hg-Sb deposit	Au-Hg-Sb deposit
	geochemical association		Au-As-Sb-Hg-Tl (Ba, Zn, Mn, Ag)	Au-As-Sb-Hg-Tl (Ba, Te, locally Zn, Cu, W, Co, Ni, Ag)
	zoning		weakly manifested	weakly manifested; pathfinder elements are locally exhibit zoning both vertically or laterally (Heitt et al., 2003; Patterson, Muntean, 2011)
	ore fluids		moderate temperature (110–215°C), relatively low salinity (4-9 wt% NaCl equiv.), aqueous liquid-rich, CO_2-bearing, CH_4 is minor	moderate temperature (100-300°C), relatively low salinity (0.5-8 wt% NaCl equiv.), aqueous liquid-rich, CO_2-bearing; in some cases with petroleum (Nutt et al., 2003)
	fluid reservoirs		magmatic fluid; deep mantle-derived fluid; catagenic and contact-metamorphic waters; meteoric water	magmatic fluid; deep mantle-derived fluid; meteoric water; metamorphic waters
	depth		1.5-2 km	<3 km (0.3-5 km)
Orebodies	morphology		contour are irregular and not visible (assay boundary): stratiform, lens-like, irregular-shaped, rarer discordant vein zones	contour are irregular and not visible (assay boundary): strata-bound, lens-like; discordant breccias zone, irregular-shaped rarer isometric, stock, carrot, T-shape, discordant vein zones
	macroscopic occurrence		fine-disseminated Fe-As sulphide minerals	fine-grained Fe-As sulphide minerals
Minera-logical (unoxidised ore)	ore minerals	main	pyrite, arsenian pyrite, realgar, orpiment, arsenopyrite	pyrite, arsenian pyrite, realgar, orpiment, arsenopyrite, marcasite
		minor	native gold, marcasite, stibnite, pyrrhotite, cinnabar, arsenic, lölingite, locally tennantite-tetrahedrite, sphalerite, galena, magnetite	native gold, pyrrhotite, stibnite, cinnabar, arsenic, locally sphalerite, galena, chalcopyrite, bornite, digenite, tetrahedrite, magnetite, hubnerite, stannite, millerite
		rare	Tl, Hg, Cu, Pb, Mn, Ag, Fe sulphides and sulphosalts, Hg, Bi, Ag, Pb sulphides and tellurides, aurostibite, calaverite	Tl, Hg, Cu, Pb, Ag sulphides and sulphosalts, Hg- and other tellurides, auricupride
		Py, Apy zoning	strong	strong
	vein mineral assemblage		quartz, calcite, barite, dolomite, ankerite, fluorite, layered alumino-silicates	quartz, calcite, barite, organic carbon, dolomite, ankerite, siderite, fluorite, layered alumino-silicates
	gold occurrence (primary ore)		micron-submicron gold in arsenian pyrite; microscopic gold rarely occurs as inclusion gold, fracture gold, intergranular gold; gold occurrence in clay minerals is very probable; that in carbonaceous matter is unclear	micron-submicron gold in arsenian pyrite is dominant; gold occurring in As-bearing minerals, carbonaceous and clay minerals as submicroscopic gold; microscopic gold occurs as inclusion gold, fracture gold, intergranular gold
Supergene features			Fe and Mn oxides, clay minerals, jarosite, free gold, copper, cuprite, acanthite; karst with spelean calcite	Fe oxides, clay minerals, alunite, jarosite, free gold; locally arsenolite, ilsemanite, conichalcite, copper, chrysocolla, cuprite, chalcocite, malachite, diverse phosphates and vanadates; karst with spelean calcite (Barton et al., 2018)

Lead isotopic composition for the Vorontsovka sulphides suggest mixing of mantle and crustal lead sources. The small input of radiogenic ^{206}Pb occurs during the final sulphide mineralising stage probably as a result of influence of the late phase of the Auerbakh pluton. 398-388 Ma Pb-Pb model ages for the sulphides coincide with the Ar-Ar age of hydromica from the late gold-arsenic assemblage 391.1 ± 4.9 Ma.

In the Early Devonian, due to intrusion of the Auerbakh pluton of the shoshonite series at a depth of <5 km, skarn magnetite ore with subordinate late sulphides was formed in the Vorontsovka area. Our genetic model for the Vorontsovka deposit suggests that main gold-arsenic Carlin-style mineralisation stage overprinted barren distal skarn is coeval with (or immediately after) emplacement of the late phase of the Auerbakh volcano-plutonic complex. Global Vorontsovka mineralisation trend corresponded to TPX-evolution with decreasing temperature, pressures, sulphur and oxygen fugacity.

Specific Carlin-style features of the Vorontsovk deposit are as follows: the paleo-continental margin and trust-related position; causing high-K/shoshonitic igneous activity; the fine-disseminated sulphide mineralisation in the highly brecciated carbonate-clastic sequence; jasperoid and argillic alteration accompaining gold orebodies with assay boundaries; multiple fluid source; Au-As-Hg-Tl geochemical association; the abundance of As-sulphides, along with As-Fe-sulphides belonging to the category of the main minerals; the occurrence of Hg-, Tl-sulphides and sulphosalts; the association of gold with arsenian pyrite and arsenopyrite overgrowing previously forming pyrite; and the predominance of submicroscopic gold in the ores. A LA-ICP-MS analysis of pyrite confirms that elevated concentrations of Au regularly correlate with higher contents of As, Ag, Sb or Tl.

ACKNOWLEDGMENTS

We thank the managers and geological team of CJSC Gold of Northern Urals (Polymetal) for their assistance during fieldwork. We are grateful to N.V. Trubkin, E.V. Kovalchuk, V.D. Abramova, T.A. Velivetskaya, Yu.L. Ronkin, E.A. Naumov, and A.V. Travin for the analytical procedures. The constructive comments of S. Soloviev and the technical assistance of P. Kaylachakov, O. Azovskova, M. Rovnushkin, and R. Vykhristenko are also appreciated. Klaus Mezger, Alexandre Tarantola, and two anonymous reviewers are thanked for their very useful comments that helped to improve the manuscript. This study was supported by the Russian Scientific Foundation grant No. 14-17-00693-P.

The following are the supplementary data related to this article:

Appendix A. Samples and analytical methods

Context of field study and sampling; details of laboratory procedures: ore petrography, electron microprobe, SEM, LA-ICP-MS, fluid inclusion study, sulphur, carbon, oxygen, hydrogen, strontium, argon and lead isotope analysis.

Appendix B. Supplementary materials

Sequence of mineral parageneses with total list of ore minerals; EPMA data of chemical composition of sulphosalts and some co-existing sulphides; data Pb isotope study of sulphides and some related age constrains; compilation data on fluid inclusion study for Carlin-type and Carlin-like deposits; comparison of Vorontsovka and Carlin-type (Nevada and Yukon) deposits. Supp. Figures include profiles and maps of LA-ICP-MS study of pyrite and arsenopyrite; results of Ar-Ar dating of ore-related hydromica; correlation scheme of isotope dating of mineralisation and some magmatic suits.

Supplementary data to this article can be found online at https://doi.org/

REFERENCES

Baklaev, J.P., Usenko, I.A., 1989. Auerbach-Turya ore field. In: Skarn-Magnetite Formation of the Urals. Middle and South Urals. Sverdlovsk: UrB AS USSR, pp. 25–58 (in Rus.).

Barannikov, A.G., Asoskova, O.B., Ravnushkin, M.J., Gottman, A.A., Smagin, I.V., 2016. Mesozoic ore-bearing karst of Vorontsovka gold deposit, North Urals. Ores and Metals (2), 84–99 (in Rus.).

Barannikov, A.G., Ugryumov, A.N., 2003. Problems of endogenous gold ore genesis of the Mesozoic of the Urals. Lithosphere. (1), 13–26. (in Rus.)

Baranov, E.N., Grinenko, L.N., Pavlov, G.P., 1985. Sulphur isotopic composition of pyrites of skarn-magnetite deposits of the Urals. Geochem. Intern. (12), 1713–1722. (in Rus.)

Barton, I., Ahn, J., Lee, J., 2018. Mineralogical and metallurgical study of supergene ores of the Mike Cu-Au(-Zn) deposit, Carlin trend, Nevada. Hydrometallurgy 176, 176–191.

Begetnev, S.V., 1999. Gold-bearing jasperoids of Auerbakh ore cluster and its importance for prospecting. Ph.D. thesis. Yekaterinburg (in Rus.).

Barber, K., 2015. Geology, Alteration, Geochemistry, and Paragenesis of the Vista Vein Shear Zone Deposit, Humboldt County, Nevada. Master thesis. Uni. Nevada, Reno. 202 pp.

Berger, B.R., Bagby, W.C., 1991. The geology and origin of Carlin-type gold deposits. In: Foster R.P., ed. Gold Metallogeny and Exploration, 210-48. Blackie, Glasgow.

Berger, V.I., Theodore, T.G., 2005. Implications of stratabound Carlin-type gold deposits in Paleozoic rocks of north-central Nevada. In: Rhoden H.N., Steininger R.C., Vikre P.G., eds. Geol. Soc. Nevada Symp. 2005: Window to the World, Reno, Nevada, pp. 43–78.

Berger, V.I., Mosier, D.L., Bliss, J.D., Moring, B.C., 2014. Sediment-Hosted Gold Deposits of the World-Database and Grade and Tonnage Models. Open-file report 2014-1074. 2014. Virginia, Reston: U.S. Geological Survey. 46 p.

Bettles, K., 2002. Exploration and geology, 1962 to 2002, at the Goldstrike property, Carlin trend, Nevada. In: Integrated Methods for Discovery: Global Exploration in the Twenty-First Century, Soc. Econ. Geol. Spec. Publ. 9, pp. 275–298.

Bobrov, V.N., 1991. Metasomatic and accompanying gold ore zoning in the precious metal deposit. In: Ore-bearing metasomatic formations of the Urals. Sverdlovsk: Ural Brunch Acad. Sci. SSSR, pp. 44–46. (in Rus.)

Bobrov, V.N. Vorontsovka Treasure. Searches and Discoveries, 2013. Karpinsk: Publ. house "Prospect". 32 p. (in Rus.)

Bochkarev, V.V., Yazeva, R.G., 2000. Subalkaline Magmatism of the Urals. Ekaterinburg: UrO RAN. 256 p. (in Rus.)

Bodnar, R.J., Lecumberri-Sanchez, P., Moncada, D., Steele-Maclnnes, P., 2014. Fluid Inclusions. In: Hydrothermal Ore Deposits. Reference Module in Earth Systems and Environmental Sciences. Treatise on Geochemistry. 2nd Edition. Elsevier. pp. 119–142.

Borisenko, A.S., 1977. Cryometric analysis of salt composition in vapour-fluid inclusions in minerals. Geol. Geofiz. 8, 16–27.

Bowman, J.R., 1998. Stable-isotope systematics in skarns. In: Lentz, D.R. (Ed.) Mineralized

Intrusion-related Skarn Systems, Short course vol. 26. Mineralogical Association of Canada, pp. 1–49.

Cheremisin, A.A., Zlotnik-Khotkevich, A.G., 1997. Vorontsovka gold deposit. Ores and Metals 1, 59–70 (in Rus.).

Chernyshev, I.V., Vikent'ev, I.V., Chugaev, A.V., Shatagin, K.N., Moloshag, V.P., 2008. Sources of material for massive sulfide deposits in the Urals: evidence from the high-precision MC-ICP-MS isotopic analysis of Pb in galena. Dokl. Earth Sci. 418, 178–183.

Cline, J.S., Hofstra, A.A., 2000. Ore-fluid evolution at the Getchell Carlin-type gold deposit, Nevada, USA. Europ. J. Mineral. 12(1), 195–212.

Cline, J.S., Hofstra, A.H., Muntean, J.L., Tosdal, R.M., Hickey, K., 2005. Carlin-type deposits in Nevada: critical geological characteristics and viable models. Econ. Geol. 100, 371–405

Cohen, K.M., Finney, S.C., Gibbard, P.L., Fan, J.-X., 2013. The ICS International Chronostratigraphic Chart. Episodes 36, 199–204.

Cunningham, C.G., Ashley, R.P., Chou, I.M., Zushu, H., Chaoyuan, W., Wenkang, L., 1988. Newly discovered sedimentary rock-hosted disseminated gold deposits in the People's Republic of China. Econ. Geol. 83(7), 1462–1467.

Demény, A., Sitnikova, M., Karchevsky, P., 2004. Stable C and O isotope compositions of carbonatite complexes of the Kola Alkaline Province: phoscorite–carbonatite relationships and source compositions. In: Wall F., Zaitsev A.N. (eds) Phoscorites and carbonatites from mantle to mine: the key example of the Kola Alkaline Province. The Mineralogical Society, London, pp. 407–431.

Doe, B.R., Zartman, R.E., 1979. Plumbotectonics. In: Barnes, H.L. (Ed.), Geochemistry of Hydrothermal Ore Deposits, 3rd edn. Wiley, New York, pp. 22–70.

Dymkin, A.M., Koroteev V.A., eds., 1990. The Main Ore Geological and Geochemical Systems. Moscow: Nauka-Publ. 269 p.

Einaudi, M.T., Meinert, L.D., Newberry, R.J., 1981. Skarn deposits. Econ. Geol. 75th Anniv. Vol., pp. 317−391.

Emsbo P., Groves D.I., Hofstra A.H., Bierlein F.P., 2006. The giant Carlin gold province: A protracted interplay of orogenic, basinal, and hydrothermal processes above a lithospheric boundary. Mineral. Dep. 41, 517–525.

Fershtater, G.B., Malakhova, L.V., Borodina, N.C. et al. Eugeosynclinal gabbro-granitoid series. Moscow: Nauka Publ., 1984. 264 p. (in Rus.)

Faure, G., 1986. Principles of Isotope Geology, second ed. John Wiley and Sons, New York.

Grabezhev, A.I., Ronkin Yu, L., Puchkov, V.N., Gerdes, A., Rovnushkin, M.Y., 2014. Krasnotur'insk skarn copper ore field, northern Urals: the U–Pb Age of orecontrolling diorites and their place in the regional metallogeny Dokl. Earth Sci. 456 (2), 641–645.

Groff, J.A., Campbell, A.R., Norman, D.I., 2002. An evaluation of fluid inclusion microthermometric data for orpiment-realgar-calcite-barite-gold mineralization at the Betze and Carlin mines, Nevada. Econ. Geol. 97(6), 1341–1346.

Groff, J.A., 2018. Distinguishing generations of quartz and a distinct gas signature of deep high-

grade Carlin-type gold mineralization using quadrupole mass spectrometry. Ore Geology Rev. 95, 518–536.

Gryaznov, O.N., Vakhrushev, S.N., 1997. Gold-argillicola formation of the Urals. Ores and Metals (2), 73–84 (in Rus.).

Gu, X.X., Zhang, Y.M., Li, B.H., Dong, S.Y., Xue, C.J., Fu, S.H., 2012. Hydrocarbon- and ore-bearing basinal fluids: a possible link between gold mineralization and hydrocarbon accumulation in the Youjiang basin, South China. Mineral. Dep. 47, 663–682.

Heitt, D.G., Dunbar, W.W. Thompson, T.B., Jackson, R.G., 2003. Geology and Geochemistry of the Deep Star Gold Deposit, Carlin Trend, Nevada. Econ. Geol. 98, 1107–1136.

Herrington, R., Zaykov, V.V., Maslennikov, V.V., Brown, D., Puchkov, V.N., 2005. Mineral deposits of the Urals and links to geodynamic evolution. Econ. Geol. 100th Anniv. Vol., pp. 1069–1095.

Hofstra, A.H., Cline, J.S., 2000. Characteristics and models for Carlin-type gold deposits. Rev. Econ. Geol. 13, 163–220.

Hofstra, A.H., Snee, L.W., Rye, R.O., Folger, H.W., Phinisey, J.D., Loranger, R.J., Dahl, A.R., Naeser, C.W., Stein, H.J., Lewchuck, M., 1999. Age constraints on Jerritt Canyon and other Carlin-Type gold deposits in the western United States-relationship to mid-Tertiary extension and magmatism. Econ. Geol. 94, 769–802.

Hoefs, J., 1997. Stable Isotope Geochemistry. Springer-Verlag, Berlin.

Hronsky, J.M.A., Groves, D.I., Loucks, R.R., Begg, G.C., 2012. A unified model for gold mineralisation in accretionary orogens and implications for regional-scale exploration targeting methods. Miner Deposita. 47, 339–358.

Humphreys, E.D., 1995. Post-Laramide removal of the Farallon slab, western United States. Geology 23, 987–990.

Jaffrés, J.B.D., Shields, G.A., Wallmann, K., 2007. The oxygen isotope evolution of seawater: A critical review of a long-standing controversy and an improved geological water cycle model for the past 3.4 billion years. Earth-Sci. Rev. 83, 83–122.

Johnson, C.L., Dilles, J.H., Kent, A.J.R., Farmer, L.P., 2015. Petrology and geochemistry of the Emigrant Pass volcanics, Nevada: implications for a magmatic-hydrothermal origin of the Carlin gold deposits. In: Pennell W.M., Garside L.J. (eds) New Concepts and Discoveries, vol 1. Geol. Soc. Nevada 2015 Symposium, DEStech Publications Inc., Lancaster, pp. 391–408.

Kesler, S.E., Riciputi, L.C., Ye, Z.J., 2005. Evidence for magmatic origin for Carlin-type gold deposits: isotopic composition of sulfur in the Betze-Post-Screamer deposit, Nevada, USA. Miner. Deposita 40, 127–136.

Kholmogorov, A.I, Yakovlev, Ya.V., Zhdanov, Yu.Ya., 1977. Typochemistry of arsenopyrite of East Yakutia. In: Minerals of Endogenous Formations of Yakutia. Yakutsk, pp. 67–77.

Kolonin, G.R., Palyanova, G.A., Shironosova, G.P., 1988. Stability and solubility of arsenopyrite in hydrothermal solutions. Geochemistry Intern. (6), 843–855.

Koroteev, V.A., de Boorder, H., Necheukhin, V.M., Sazonov, V.N., 1997. Geodynamic setting of the mineral deposits of the Urals. Tectonophys. 276, 291–300.

Korzhinsky, D.S., Pertsev, N.N., Zotov, I.A., 1984. Transmagmatic fluids and magmatogenic ore formation. A problem of mantle ore sources. Proc. Sixth IAGOD symp. Stuttgart. Vol. 1. pp. 131–138.

Krasnobaev, A.A., Fershtater, G.B., Bogomolov, E.S., et al., 2007. Auerbah granitoid massif: zircons, age, polichrono. Yearbook 2006 Institute of Geology and Geochemistry. Information Collection of Scientific Papers. IGG UB RAS, Yekaterinburg, pp. 191–196 (in Rus.).

Kuzmin, M.I., 1985. Geochemistry of Magmatic rocks of Phanerozoic Mobile Belts. Novosibirsk: Nauka Publ. 198 p. (in Rus.)

Large, S.J.E., Bakker, E.Y.N., Weis, P., Wälle, M., Ressel, M., Heinrich, C.A., 2016. Trace elements in fluid inclusions of sediment-hosted gold deposits indicate a magmatic-hydrothermal origin of the Carlin ore trend. Geology. 44(12), 1015–1018.

Lindblom, S., 1991. Organic matter and gold deposition in disseminated gold deposits in Nevada. In: Source, Transport and Deposition of Metals, eds. M. Pagel, J. Leroy, Balkema, Rotterdam. pp. 553-556.

Luo, Z.-H., Mo, X.-X, Lu, X.-X., Chen, B.-H., Ke, S., Hou, Z.Q., Jiang, W., 2007. Metallogeny by trans-magmatic fluids – theoretical analysis and field evidence Earth Science Frontiers, 14(3), 165–183.

Malakhov, L.V., Churilin, N.S., 1972. Basalt granitoids and their comagmatics in the Tagil trough (Middle Urals). Questions of Petrology of Granitoids of the Urals. Sverdlovsk: UrB AS USSR, pp. 33–75 (in Rus.).

Meffre, S., Large, R.R., Steadman, J.A., Gregory, D.D., Stepanov, A., Kamenetsky, V., Ehrig, K., Scott, R.J., 2016. Multi-stage enrichment processes for large gold-bearing ore deposits, Ore Geol. Rev. 76, 268–279.

Minina, O.V., 1994. Auerbah complex ore-magmatic system in the Middle Urals. Otechestvennaya Geol. 7, 17–23 (in Rus.).

Murzin, V.V., Naumov E.A., Azovskova O.B., Varlamov D.A., Rovnushkin M.Yu., Pirajno F., 2017. The Vorontsovskoe Au-Hg-As ore deposit (Northern Urals, Russia): Geological setting, ore mineralogy, geochemistry, geochronology and genetic model. Ore Geol. Rev. 85, 271–298.

Murzin, V.V., Pokrovsky, P.V., Molosag, V.P., 1981. Mercury in native gold of the Urals and its typomorphic significance. Geology Ore Depos. (4), 86-91 (in Rus.).

Murzin, V.V., Sazonov, V.N., 1996. Mineral assemblages and the conditions for the formation of sulphide gold mineralisation at Turya-Auerbah ore cluster (Urals). Ural Branch Rus. Acad. Sci., Yekaterinburg (in Rus.).

Murzin, V.V., Sazonov, V.N., 1999. Gold-bearing mineral assemblages in the copper and iron skarn deposits of the Tur'insk-Auyerbakh ore field and their formation condition (Urals, Russia). Geology Ore Depos. 41 (4), 308–321.

Murzin, V.V., Sazonov, V.N., Ronkin, Y.L., 2010. Model for formation of Vorontsovskoe gold deposit in the Urals (Carlin type): new data and problems. Lithosphere 6, 66–73 (in Rus.).

Muntean, J.L., Cline, J.S., Simon, A.C., Longo, A.A., 2011. Magmatic hydrothermal origin of

Nevada's Carlin-type gold deposits. Nature Geos. 4, 122–127.

Muntean, J.L., Bonner, W., Hill, T., 2017. Carlin-style gold-silver mineralization at the Cove deposit in Nevada, USA: possible missing link between Carlin-type gold deposits and magmatic-hydrothermal systems. Mineral Resources to Discover. 14th SGA Meet. Canada, Quebec, vol. 1, pp. 71–74.

Narkisova, V.V., 2005. Petrochemistry of Late Ordovician – Early Devonian basaltoids of southern part of the Middle Urals (according to data from Ural superdeep borehole and near-borehole space). Lomonosov State uni. Moscow, Ph.D. thesis (in Rus.).

Naumov, E.A., Borovikov, A.A., Borisenko, A.S., Zadorozhniy, M.V., Murzin, V.V., 2002. Physicochemical conditions of formation of epithermal gold-mercury deposits. Geol. Geofiz. 43, 1003–1013.

Norby, J., Orobona, M., 2002. Geology and mineral systems of the Mike deposit. In: Thomson, T. (Ed.), Gold Deposits of the Carlin Trend: Nevada Bureau of Mines and Geology Bulletin 111, pp. 143–167.

Nosova, A.A., Sazonova, L.V., Narkisova, V.V., Bubnov, S.N., Gurbanov, A.G., 2000. Petrology of calc-alkaline volcanic rocks of the Pavda complex, Tagil depression, based on a study of zonal clinopyroxene: Evidence from materials recovered by the Ural superdeep hole. Petrology 8(2), 161–176.

Nosova, A.A., Sazonova, L.V., Narkisova, V.V., Simakin, S.G, 2002. Minor elements in clinopyroxene from Paleozoic volcanics of the Tagil island arc in the Central Urals. Geochem. Intern. 40(3), 219–232.

Nutt, C.J., Hofstra, A.H., 2003. Alligator Ridge District, East-Central Nevada: Carlin-type gold mineralization at shallow depths. Econ. Geol. 98, 1225–1241.

Ohmoto, H., Rye, R.O., 1979. Isotopes of sulphur and carbon. In: Barnes, H.L. (Ed.), Geochemistry of Hydrothermal Ore Deposits. J. Willy., Sons, New York, pp. 509–567.

Oppliger, G. L., Murphy, J. B., Brimhall, G. H., Jr., 1997. Is the ancestral Yellowstone hotspot responsible for the Tertiary "Carlin" mineralization in the Great Basin of Nevada? Geology 25, 627–630.

Perkova, R.I., 1975. Sulphur Isotope Composition of Sulphides and Some Problems of Genesis of the Contact-Metasomatic Deposits of Auerbakh-Turya Ore Field. Ph.D. thesis, Sverdlovsk (in Rus.).

Patterson, L.M., Muntean, J.L., 2011. Multi-element geochemistry across a Carlin-type gold district: Jerritt Canyon, Nevada. Geol. Soc. Nevada, Symp., vol. 2, pp.1119–1151.

Puchkov V.N., 2009. The diachronous (step-wise) arc–continent collision in the Urals. Tectonophysics 479, 175–184.

Puchkov, V.N., 2010. Geology of Urals and Cis-Urals (actual problems of stratigraphy, tectonics, geodynamics and metallogeny). DesignPoligraphService, Ufa (in Rus.).

Radtke, A.S., 1985. Geology of the Carlin gold deposit, Nevada. U.S. Geol. Surv. Prof. Pap. No 1267. 263 pp.

Radtke, A.S., Rye, R.O., Dickson, F.W., 1980. Geology and stable isotope studies of Carlin gold

deposit, Nevada. Econ. Geol. 75(5), 641–672.

Rakhov, E.V., 1999. The ore-bearing breccia of Vorontsovka deposit: structure, genesis and role in the formation of gold mineralisation, Ph.D. thesis, Yekaterinburg (in Rus.).

Ressel, M.W., Henry, C.D., 2006. Igneous geology of the Carlin trend, Nevada: development of the Eocene plutonic complex and significance for Carlin-type gold deposits. Econ. Geol. 101, 347–383.

Ripley, E.M., Li, C., 2003. Sulfur isotope exchange and metal enrichment in the formation of magmatic Cu-Ni-(PGE) deposits. Econ. Geol. 98 (3), 635–641.

Ronkin, Y.L., Petrov, G.A., Lepikhina, O.P., 2009. Precision Sm-Nd isotope dating of Auerbah gabbro-granite complex (North Urals). Isotopic Systems and Time of Geological Processes. Proc. IV Rus. Conf. Isotope Geochron. V. II, pp. 122–124 (St. Petersburg, (in Rus.)).

Ryskamp, E.B., Abbott, J.T., Christiansen, E.H., Keith, J.D., Vervoort, J.D., Tingey, D.G., 2008. Age and petrogenesis of volcanic and intrusive rocks in the Sulphur Spring Range, central Nevada: Comparisons with ore-associate Eocene magma systems in the Great Basin. Geosphere 4(3), 496–519.

Sazonov, V.N., Murzin, V.V., Grigoryev, N.A., Gladkovsky, B.A., 1991. Endogenous Mineralisation of Devonian Andesite Volcano-plutonic Complex (Urals). Ural Branch of the Academy of Sciences of the USSR, Sverdlovsk (in Rus.).

Sazonov, V.N., Murzin, V.V., Grigor'ev, N.A., 1998. Vorontsovsk gold deposit: an example of Carlin-type mineralization in the Urals, Russia. Geology Ore Depos. 40 (2), 139–151.

Sazonov, V.N., van Herk, A.H., de Boorder, H., 2001. Spatial and temporal distribution of gold deposits in the Urals. Econ. Geol. 96, 685–703.

Sazonova, L.V., Nosova, A.A., Narkisova, V.V., Gurbanov, A.G., Bubnov, S.N., 1997. Clinopyroxene in volcanic rocks of the Tagil depression, Ural superdeep hole. Petrology 5(5), 466–482.

Seal, R., 2006. Sulfur isotope geochemistry of sulfide minerals. Rev. Miner. Geoch. 61, 633–677.

Shervais, J.W., 2001, Birth, death, and resurrection: The life cycle of suprasubduction zone ophiolites. Geochem., Geophys., Geosyst. 2, 1–45. doi: 10.1029/2000GC000080.

Sillitoe, R.H., Bonham, H.F., 1990. Sediment-hosted gold deposits: Distal products of magmatic-hydrothermal systems. Geology 18, 157–161.

Soloviev, S.G., 2014a. The Metallogeny of Shoshonitic Magmatism (Volume I). Scientific World Publ., Moscow. 528 pp. (in Rus).

Soloviev, S.G., 2014b. The Metallogeny of Shoshonitic Magmatism (Volume II). Scientific World Publ., Moscow. 472 pp. (in Rus).

Stacey, J.S., Kramers, I.D., 1975. Approximation of terrestrial lead isotope evolution by a two-stage model. Earth Planet. Sci. Lett. 26(2), 207–221.

Su, W., Heinrich, C.A., Pettke, T., Zhang, X., Hu, R., Xia, B., 2009. Sediment-hosted gold deposits in Guizhou, China: Products of wall-rock sulphydation by deep crustal fluids. Econ. Geol. 104(1), 73–93.

Teal, L., Branham, A., 1997. Geology of the Mike gold-copper deposit, Eureka County, Nevada. SEG Guidebook 28, 257–276.

Tyukova, E.E., Voroshin, S.V., 2007. Arsenopyrite Compositions and Assemblages in Ore Deposits and Host Rocks of the Upper Kolyma River Area (Interpreting the Genesis of Sulphide Mineral Assemblages). NEISRI, Far East Branch, Rus. Acad. Sci., Magadan. 107 pp. (in Rus.).

Veizer, J., Ala, D., Azmy, K., Bruckschen, P. et al., 1999. $^{87}Sr/^{86}Sr$, $\delta^{13}C$ and $\delta^{18}O$ evolution of Phanerozoic seawater. Chem. Geol. 161, 59–89.

Vikentyev, I.V., 1996. Ore mineralization in Silurian arc-related series of Middle Urals: Metamorphic history and sources of fluids. In: Mineralization in the Caledonides. Proc. Mike Gallagher Memorial Meeting, Edinburgh, pp. 68–69.

Vikentiev, I.V., Abramova, V.D., Ivanova, Yu.N., Tyukova, E.E., Kovalchuk, E.V., Bortnikov, N.S., 2016a. Trace elements in pyrite from the Petropavlovsk gold–porphyry deposit (Polar Urals): results of LA-ICP-MS analysis. Doklady Earth Sciences 470(1), 977–981.

Vikentyev, I.V., Tyukova, E.E., Murzin, V.V., Vikent'eva, O.V., Pavlov, L.G., 2016b. Vorontsovka Gold Deposit. Geology, Gold Modes, Genesis. Ekaterinburg: Fort Dialog-Iset Publ., 204 pp. (in Rus.).

Vikentyev, I.V., Belogub, E.V., Novoselov, K.A., Moloshag, V.P., 2017. Metamorphism of volcanogenic massive sulphide deposits of the Urals. Ore geology. Ore Geology Rev. 85, 30–63. DOI: 10.1016/j.oregeorev.2016.10.032.

Yakubchuk, A., 2017. Evolution of the Central Asian Orogenic Supercollage since Late Neoproterozoic revised again. Gondwana Res. 47, 372–398.

Yazeva, R.G., Bochkarev, V.V., 1996. Silurian island arc of the Urals: structure, evolution and geodynamics. Geotectonics 29, 478-489.

Yazeva, R.G., Puchkov, V.N., Bochkarev, V.V., 1989. Relics of the active continental margin in the Urals. Geotectonics 23, 252–259.

Zagrudinna, I.A., 1986. Sulphur isotopic composition of rocks and ores from the area of the Ural superdeep borehole. In: Value of Isotopic Studies to Improve the Efficiency and Quality of Geological Prospecting, pp. 35-42 (in Rus.).

Zharikov, V.A., 1970. Skarns. Int. Geol. Rev. 12, 541-559, 619-647, 760–775.

Zheng, Y.F., 1993. Calculation of oxygen isotope fractionation in anhydrous silicate minerals. Geochim. Cosmochim. Acta 57, 1079–1091.

Zheng, Y.F., 1999. Oxygen isotope fractionation in carbonate and sulfate minerals. Geochem. J. 33, 109–126.

Zhong, H.R., Chao, S.W., Wu, B.X., Zhi, T.G., Hofstra, A.H., 2002. Geology and geochemistry of Carlin-type gold deposits in China. Mineral. Dep. 37, 378–392.

Fig. 1. Position of major VMS, skarn and gold deposits in the Middle and Northern Urals (tectonic base map after Puchkov, 2010). I – East Europenian platform; II – West Siberian platform.

Fig. 2. Schematic geological map of the Turya-Auerbakh ore district. Compiled using unpubl. data of Lisov (1978), Bobrov (1991) and materials of Rindzyunskaya et al. (1995). Skarn deposits (after Podlessky, 1979): 1 – Auerbakh, 2 – Novo-Peschanka, 3 – North- and South-Peschanka, 4 – West-Peschanka, 5 – Poludenskoe, 6 – Vorontsovka Fe and North-Vorontsovka Fe, 7 – South-Vorontsovka Fe, 8 – Garevskoe, 9 – Vladykinskoe, 10 – Kakva, 11 – 34th quarter, 12 – Troitsk-Mikhaylov, 13 – Bogoslovsk and Bashmakov, 14 – Vadimo-Aleksandrovka, 15 – Nikitinskoe, 16 – Uspenskoe, 17 – Frolov, 18 – Suvorovskoe, 19 – Vasilyev, 20 – Sukhodoyskoe, 21 – Psarevskoe.

Fig 3. Schematic geological map and cross-section along line 50 of the Vorontsovka deposit, using Bobrov, 1991; Cheremisin, Zlotnik-Khotkevich, 1997, and mining geologists.

Fig. 4. Orebodies and host rock alteration in the central part of the Vorontsovka deposit (Line 50). See Fig.3 for legend. Compiling using Bobrov, 1991 and Gryaznov, Vakhrushev, 1997.

Fig. 5. Ores from the Vorontsovka deposit: (a) carbonate breccia with laminated semi-massive sulphide cement, Vr131-3; (b) layered tuff-clastic rock with disseminated of sulphides (pyrite, chalcopyrite, sphalerite, marcasite) altered and recrystallised along veinlet, Vr131-10; (c) brecciated limestone of cocarde structure with zones of carbonaceous matter and sulphide impregnation (pyrite, arsenopyrite, magnetite, pyrrhotite, native gold), Vr11-6; (d) polysulphide-carbonate-quartz vein in epidotised tuff, Vr118-1; (e) carbonate breccia, containing disseminated realgar with impregnation of gold, sulphides and thallium minerals, Vr128-1; (f) argillic altered tuff-clastic rocks, rich in thin impregnation of acicular arsenopyrite (Apy) which is intersected and cemented by native arsenic (As) (photo inset), associated with native gold, Vr1-2.

Fig. 6. Morphological features of sulphide impregnation in tuff-clastic rock (a, b) and in carbonate breccia (c, d): a, b – framboidal pyrite, Vr143-12; c – replacement of pyrite by As-pyrite and further by arsenopyrite, skarn, Vr10-17; d – pyrite replaced by arsenopyrite, gold-pyrite-realgar assemblage, Vr128-3.

Fig. 7. The polymodal distribution of As content in arsenopyrite of the Vorontsovka: (a) sulphide assemblages in tuff-clastic rock (II); (b) skarn (III); (c) complex ore samples (II+III); (d) gold-

pyrite-realgar assemblage (IV); (e) arsenopyrite of all ore types. Roman numbers refer to different arsenopyrite generations.

Fig. 8. Intergrowths of arsenopyrite (Apy) of different composition and morphology, gold-pyrite-realgar assemblage, Vr1-5: (a, b) idiomorphic crystals of arsenopyrite and a felt-like aggregate of thin needle-like arsenopyrite with abundant interstitial dissemination of native gold (Au) and needles of löllingite (Lö); (c, d) aggregates of parallel elongated zonal crystals of arsenic arsenopyrite (Apy-2) overgrew the prisms of the earlier sulphurous arsenopyrite (darker, Apy-1, see table inserted), Vr1-3; (e) löllingite in arsenopyrite (bright zone) and native gold associated with felt-like arsenopyrite, analysis 8 in table (microprobe Jeol JXA-8200, BSE; scale bar is 10 μm).

Fig. 9. Relationships between arsenopyrite (Apy), native arsenic (As), löllingite (Lö) and native gold (Au): (a) native arsenic, accompanied by gold, replaces early arsenopyrite, Vr 1-2; (b) "plate" of needle-like löllingite among aggregate of elongated arsenopyrite crystals, Vr1-5.

Fig. 10. Mineral relationships of the gold-pyrite-realgar assemblage in carbonate breccia: (a) routhierite (Rou) cements Hg-sphalerite (Sp), Vr123; (b) twinnite (Pb-sulphosalt) cements pyrite (Py), Vr-1.

Fig. 11. Trace-element and arsenic contents in pyrite of various assemblages according to LA-ICP-MS data for Vorontsovka. Dotted lines - detection limit.

Fig. 12. Native gold in the Vorontsovka deposit. The gold fineness in the Vorontsovka (a) and in nearby skarn deposits (b); (c) native gold with uneven composition, jasperoid, Vr-35; (d) interstitial forms of gold with elements of crystallographic faceting intergrown with arsenopyrite and native arsenic in sulphidised argillisite, Vr1.5/08.

Fig. 13. Binary plots for fluid inclusions in calcite of the Vorontsovka deposit: (a) homogenisation temperature (T_{hom}) vs. salinity (C_{salt}), (b) homogenisation temperature (T_{hom}) vs. eutectic temperatures (T_{eut}); square - gold-bearing jasperoid, triangle - gold-bearing limestone breccia.

Fig. 14. Sulphur isotope composition of sulphides from the Vorontsovka and pyrite from igneous rocks of Auerbakh Complex compared to major earth reservoirs (Ohmoto, Rye, 1979).

Fig. 15. Carbon and oxygen isotope composition of carbonates at the Vorontsovka gold deposit and Auerbah ore field. Fields of mantle reservoir (primary igneous carbonates; Hoefs, 1997;

Demeny et al., 2004) and sedimentary marine carbonates after Veizer et al., 1999 are also plotted on the diagram.

Fig. 16. C, O and Sr isotopic compositions of carbonates from the Vorontsovka deposit (global reservoirs after Veizer et al., 1999; Jaffrés et al., 2007).

Fig. 17. Diagram of variations in the homogenisation temperature and salinity for the fluids of Carlin-type (USA) and Carlin-like (China) gold deposits. Deposits of the Carlin type are divided upon ore-control features: – lithostratigraphic control (Carlin, Jerritt Canyon, Mercur), – tectonic control (Gold Quarry, Getchell, Chukar), – lithostructural control (Post-Betze, Twin Creeks, Meikle, Turquoise Ridge). Carlin-like deposits of China: Yata, Baidi, Banqi, Dongbeizhai, Gaolong, Gedang, Jinya, Lannigou, Mingshan, Shijia, Shuiyindong, Bojitian, Taipingdong, Zimudang. Compiled using Nash, 1972; Radtke et al., 1980; Cunningham et al., 1988; Lindblom, 1991; Hofstra, Cline, 2000; Groff et al., 2002; Zhong et al., 2002; Su et al., 2009; Gu et al., 2012; Large et al., 2016. Dashed line contours the field of the Vorontsovka fluids.

Fig. 18. Position of crystallisation fields and evolution trends of Vorontsovka sulphide mineral assemblages on diagram "temperature – $f\ S_2$". T – $f\ S_2$ evolution trends for early, skarn-polymetallic (I) and overprinting Carlin-style gold-bearing (II) mineral assemblages are shown by arrows; see table 5 for additional information. The solid lines represent equilibrium lines of sulphidation reactions, dashed lines – molar fraction of FeS in sphalerite, dash-dotted lines – content of silver in native gold (atomic fraction), the dotted lines - the atomic fraction of Fe in pyrrhotite. Abbreviations: Py – pyrite, Ccp – chalcopyrite, Po – pyrrhotite, Sp – sphalerite, Apy – arsenopyrite, Gn – galena, Stb – stibnite, Rl – realgar, Au – native gold, As – native arsenic, Mt – magnetite, Hem – hematite, Lö – löllingite, Bn – bornite, Cbn – cubanite, Pdy – polydymite, SS - sulphosalts.

Fig. 19. $^{207}Pb/^{204}Pb$ vs. $^{206}Pb/^{204}Pb$ plot for the Vorontsovka sulphides and galena of VMS deposits of the Middle-North Urals compared with the evolution curves and Stacey–Kramers isochrons (Stacey, Kramers, 1975) and Doe and Zartman (1979) growth curves for mantle, orogen and upper crust. Vorontsovka samples with model Pb-Pb ages later and younger 400 Ma are in various colours (see comments below the figure). Fields of data points for the Pb isotopic composition are discussed in the text of the paper. Dashed and dotted lines correspond to the

evolution curves and Stacey–Kramers isochrons, respectively; solid lines correspond to the Doe and Zartman growth curves. Analytical errors are 2–5 times smaller (in different coordinates) than the symbol dimension. Abbreviations for VMS deposits: S-D – San-Donato, G – Galka, Val – Valentor, Kab – Kaban (1 – vein in diorite, 2 – ore), Trn – Tarnyer, Saf – Safyanovka.

Fig. 20. Distal-magmato-hydrothermal model for the Vorontsovka deposit (Late Emsian stage).

Highlights

Carlin-style gold-realgar-stibnite (+Tl minerals) mineralisation in carbonate breccia;
mineralisation trend with decreasing temperature, pressures, sulphur and oxygen fugacity;
mixed post-magmatic, deep mantle-derived and metamorphic/meteoric fluid sources;
significant role of magmatic source of fluids and metals in ore-genesis;
three-stage Vorontsovka formation model

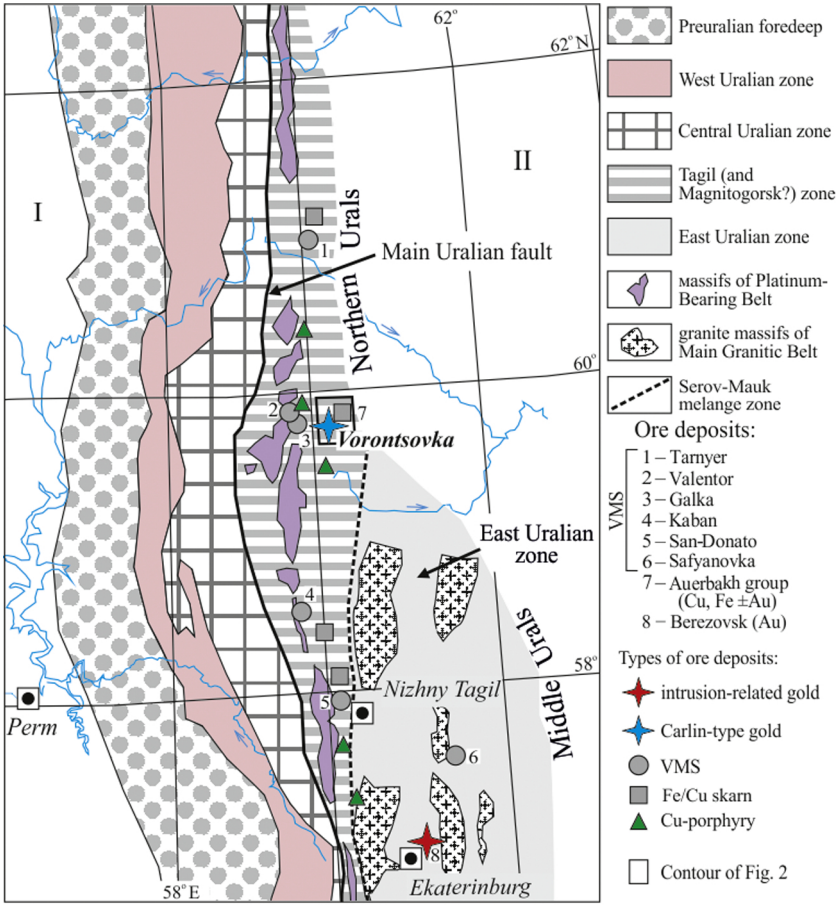
62°
62° N
60°
58°
58° E
I
II
Northern Urals
Middle Urals
Main Uralian fault
East Uralian zone
Vorontsovka
Nizhny Tagil
Ekaterinburg
Perm
1
2
3
4
5
6
7
8
Preuralian foredeep
West Uralian zone
Central Uralian zone
Tagil (and Magnitogorsk?) zone
East Uralian zone
massifs of Platinum-Bearing Belt
granite massifs of Main Granitic Belt
Serov-Mauk melange zone
Ore deposits:
VMS
1 – Tarnyer
2 – Valentor
3 – Galka
4 – Kaban
5 – San-Donato
6 – Safyanovka
7 – Auerbakh group (Cu, Fe ±Au)
8 – Berezovsk (Au)
Types of ore deposits:
intrusion-related gold
Carlin-type gold
VMS
Fe/Cu skarn
Cu-porphyry
Contour of Fig. 2

Figure 1

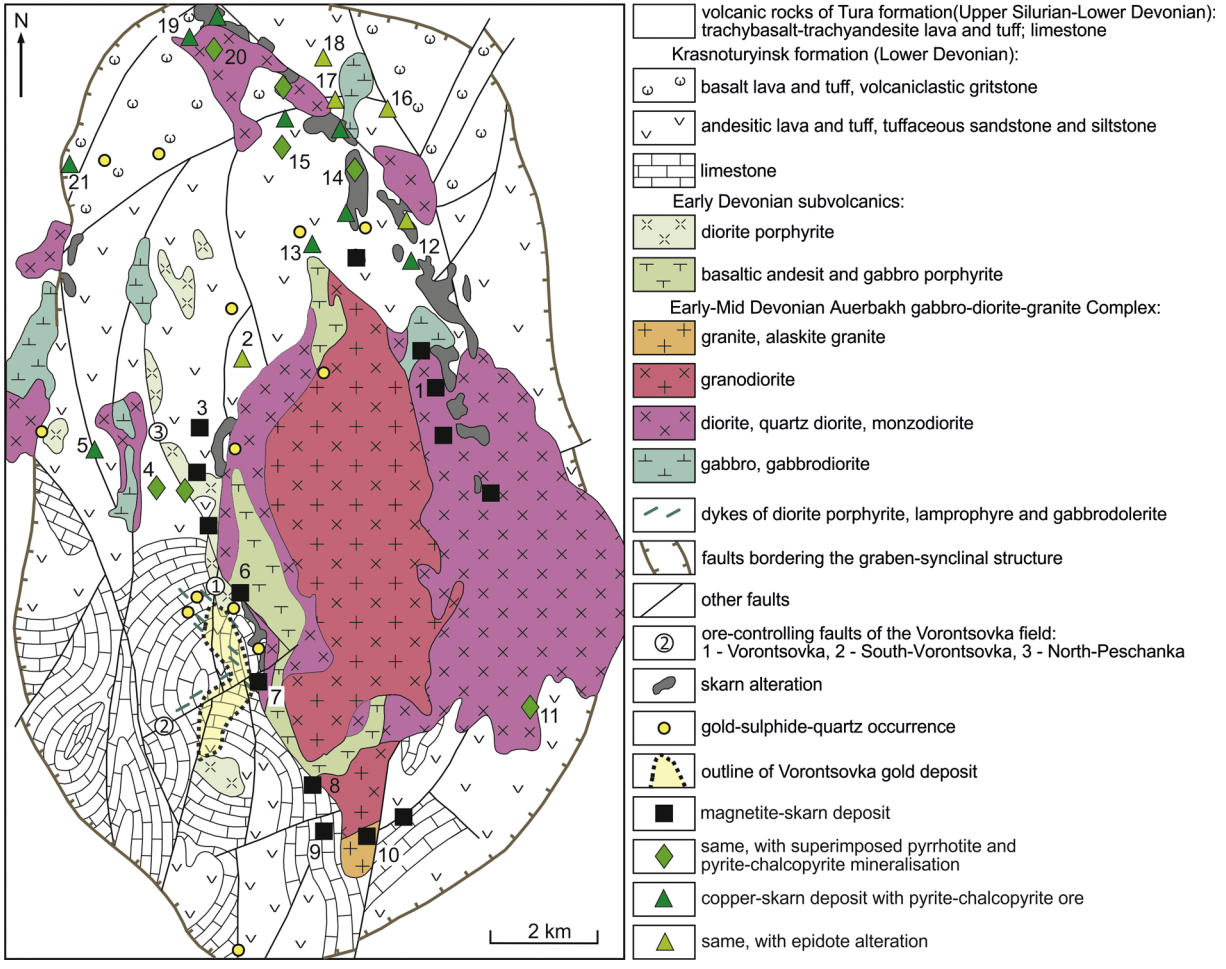
N
19
20
18
17
16
15
14
21
13
12
2
1
3
5
4
6
7
11
8
9
10
2 km
volcanic rocks of Tura formation(Upper Silurian-Lower Devonian): trachybasalt-trachyandesite lava and tuff; limestone
Krasnoturyinsk formation (Lower Devonian):
basalt lava and tuff, volcaniclastic gritstone
andesitic lava and tuff, tuffaceous sandstone and siltstone
limestone
Early Devonian subvolcanics:
diorite porphyrite
basaltic andesit and gabbro porphyrite
Early-Mid Devonian Auerbakh gabbro-diorite-granite Complex:
granite, alaskite granite
granodiorite
diorite, quartz diorite, monzodiorite
gabbro, gabbrodiorite
dykes of diorite porphyrite, lamprophyre and gabbrodolerite
faults bordering the graben-synclinal structure
other faults
ore-controlling faults of the Vorontsovka field: 1 - Vorontsovka, 2 - South-Vorontsovka, 3 - North-Peschanka
skarn alteration
gold-sulphide-quartz occurrence
outline of Vorontsovka gold deposit
magnetite-skarn deposit
same, with superimposed pyrrhotite and pyrite-chalcopyrite mineralisation
copper-skarn deposit with pyrite-chalcopyrite ore
same, with epidote alteration

Figure 2

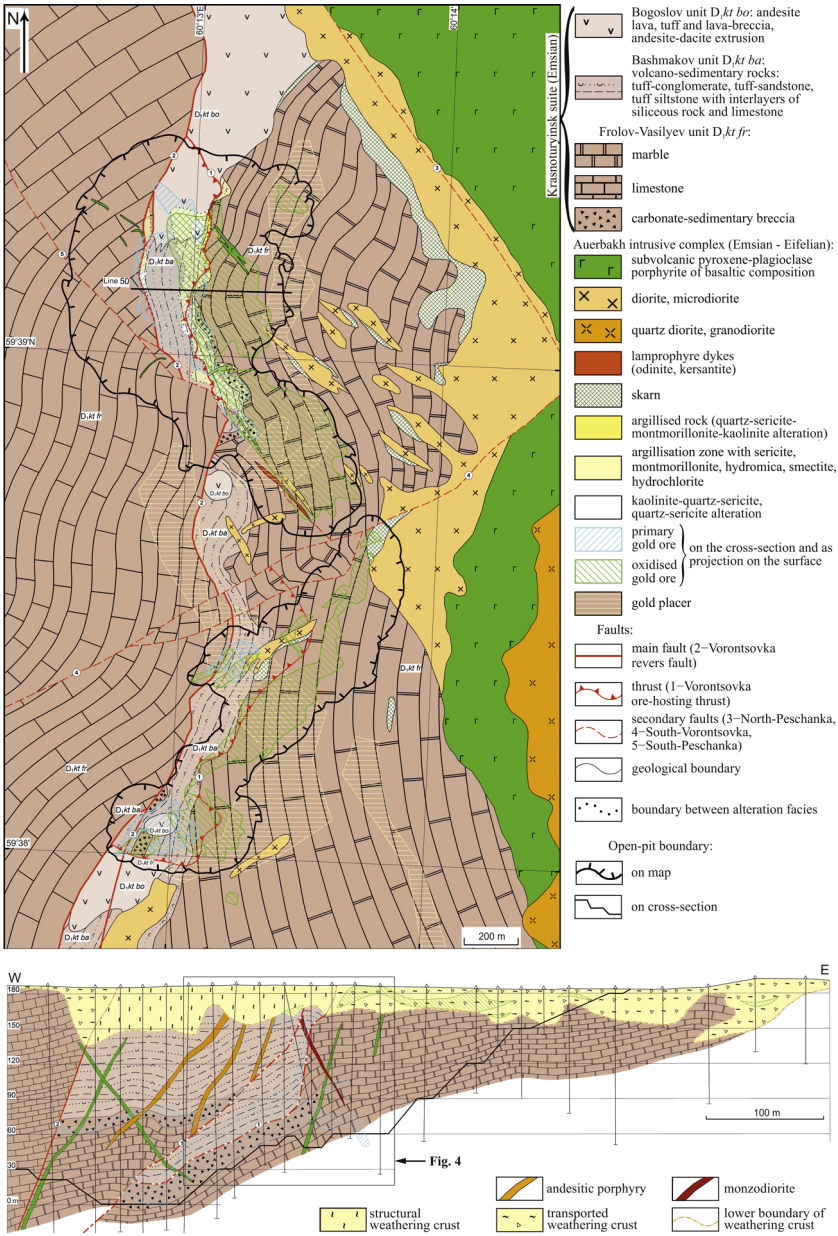
N
60°14'E
59°14'
59°39'N
59°38'
Line 50
D₂kt bo
D₂kt ba
D₂kt fr
200 m
Krasnoturyinsk suite (Emsian)
Bogoslov unit D₂kt bo: andesite lava, tuff and lava-breccia, andesite-dacite extrusion
Bashmakov unit D₂kt ba: volcano-sedimentary rocks: tuff-conglomerate, tuff-sandstone, tuff siltstone with interlayers of siliceous rock and limestone
Frolov-Vasilyev unit D₂kt fr:
marble
limestone
carbonate-sedimentary breccia
Auerbakh intrusive complex (Emsian - Eifelian):
subvolcanic pyroxene-plagioclase porphyrite of basaltic composition
diorite, microdiorite
quartz diorite, granodiorite
lamprophyre dykes (odinite, kersantite)
skarn
argillised rock (quartz-sericite-montmorillonite-kaolinite alteration)
argillisation zone with sericite, montmorillonite, hydromica, smectite, hydrochlorite
kaolinite-quartz-sericite, quartz-sericite alteration
primary gold ore
oxidised gold ore
on the cross-section and as projection on the surface
gold placer
Faults:
main fault (2−Vorontsovka revers fault)
thrust (1−Vorontsovka ore-hosting thrust)
secondary faults (3−North-Peschanka, 4−South-Vorontsovka, 5−South-Peschanka)
geological boundary
boundary between alteration facies
Open-pit boundary:
on map
on cross-section

W
E
180
150
120
90
60
30
0 m
100 m
Fig. 4
structural weathering crust
andesitic porphyry
transported weathering crust
monzodiorite
lower boundary of weathering crust

Figure 3

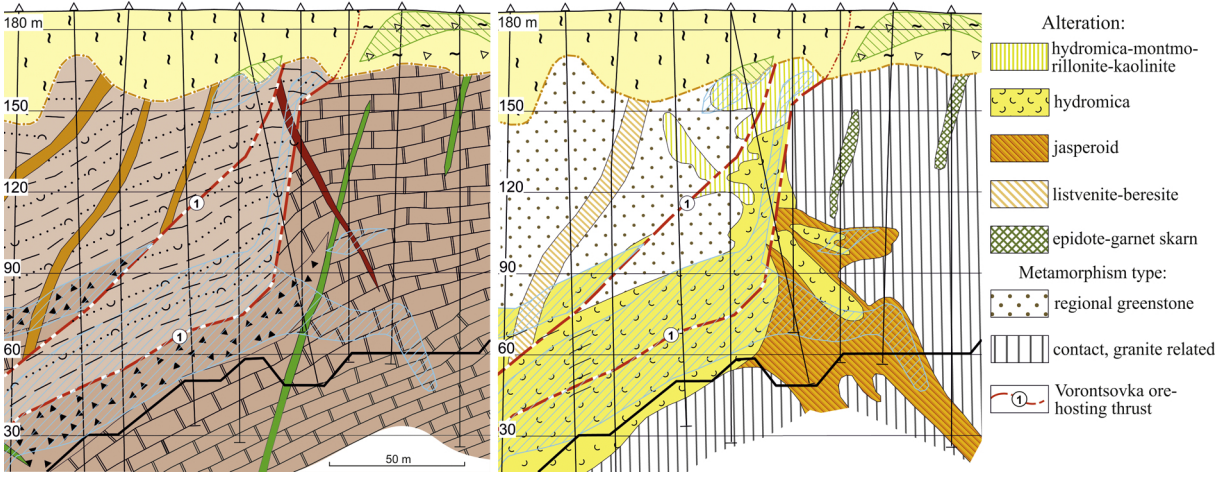
180 m
150
120
90
60
30
50 m
1
Alteration:
hydromica-montmo-
rillonite-kaolinite
hydromica
jasperoid
listvenite-beresite
epidote-garnet skarn
Metamorphism type:
regional greenstone
contact, granite related
Vorontsovka ore-
hosting thrust

Figure 4

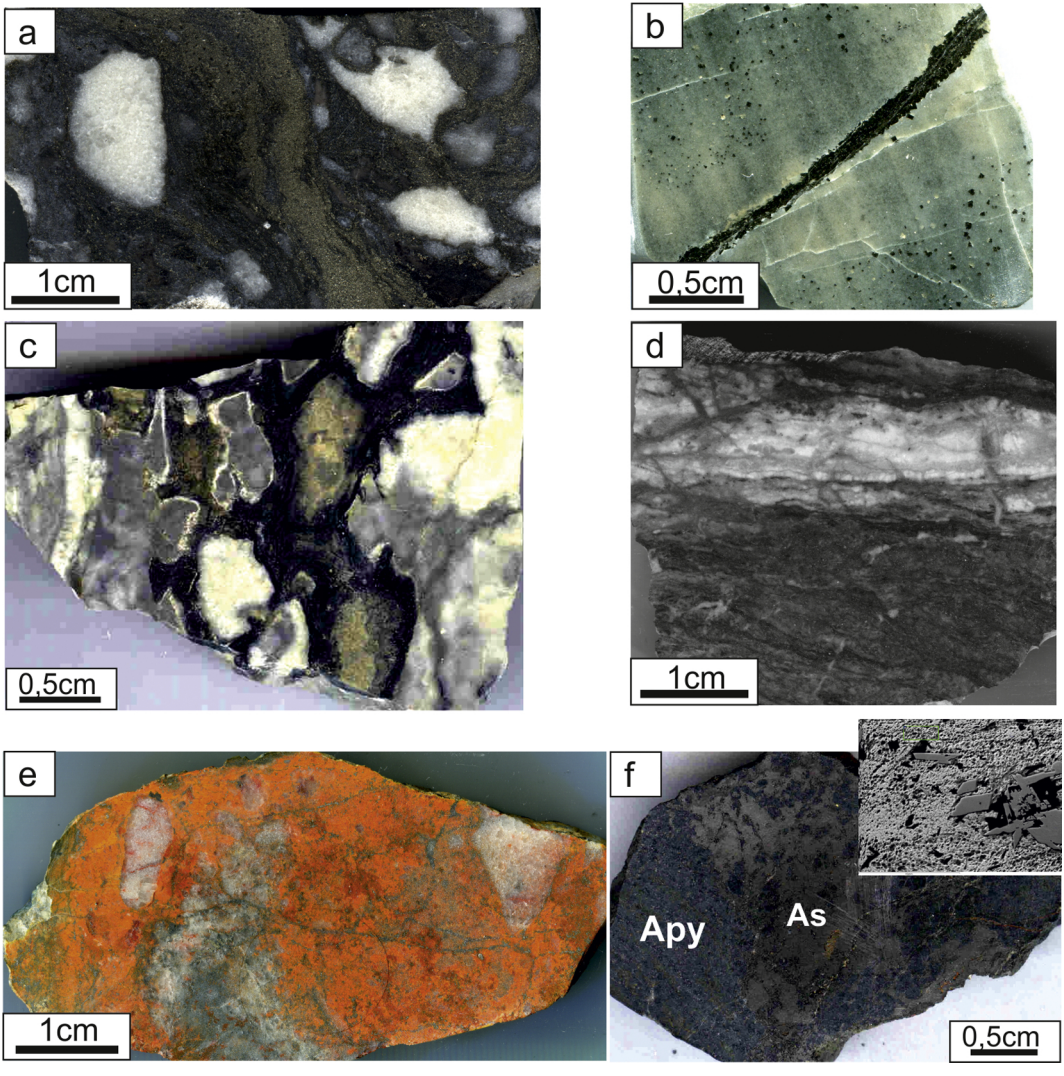

Figure 5

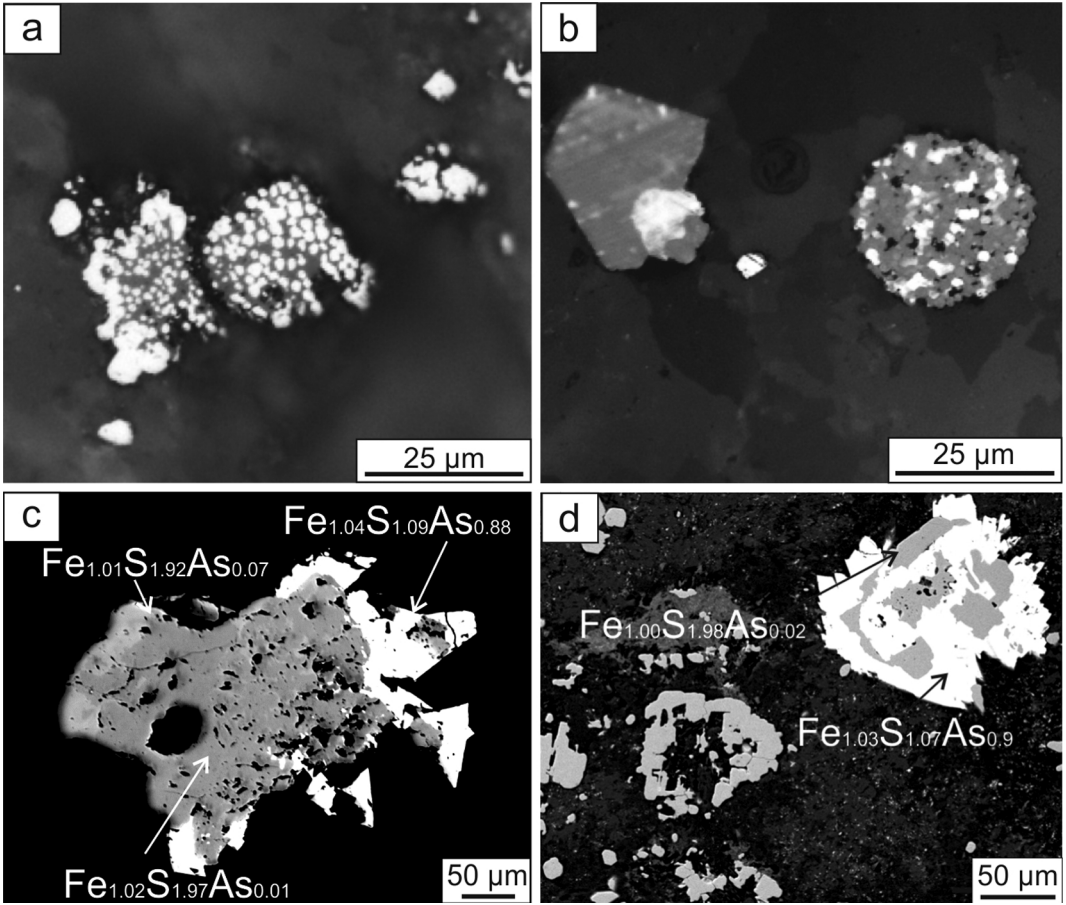
a
25 µm
b
25 µm
c
Fe1.04S1.09As0.88
Fe1.01S1.92As0.07
Fe1.02S1.97As0.01
50 µm
d
Fe1.00S1.98As0.02
Fe1.03S1.07As0.9
50 µm

Figure 6

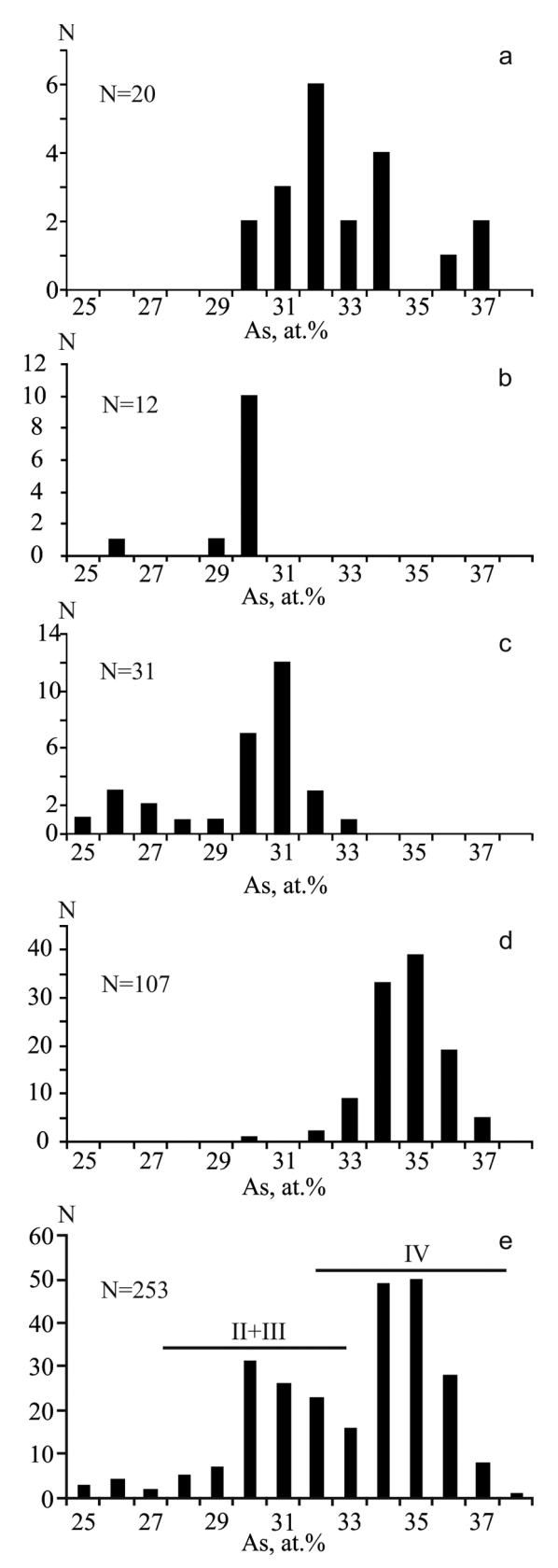

Figure 7

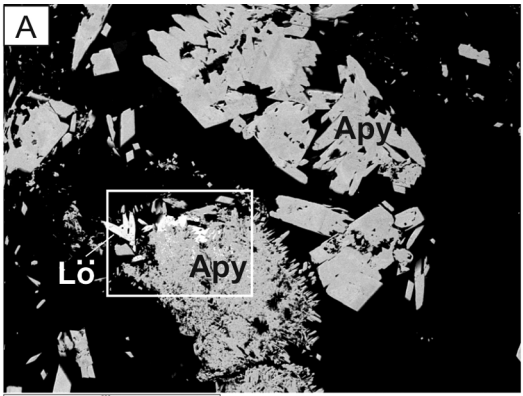

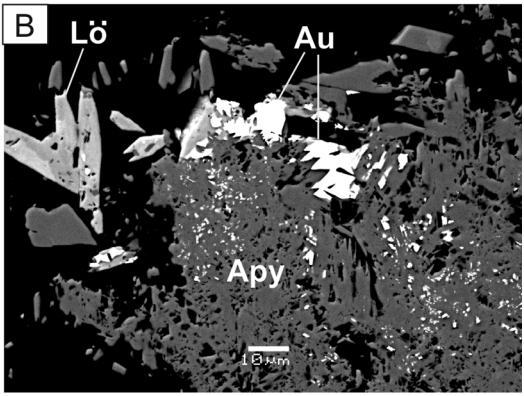

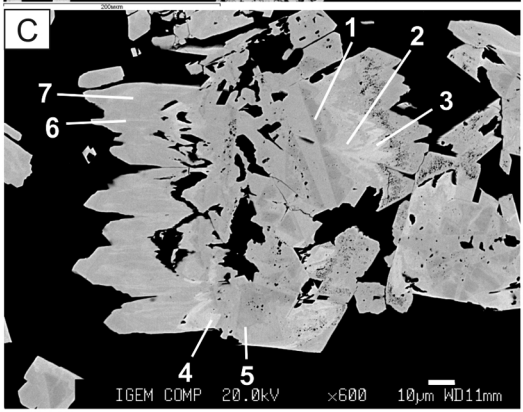

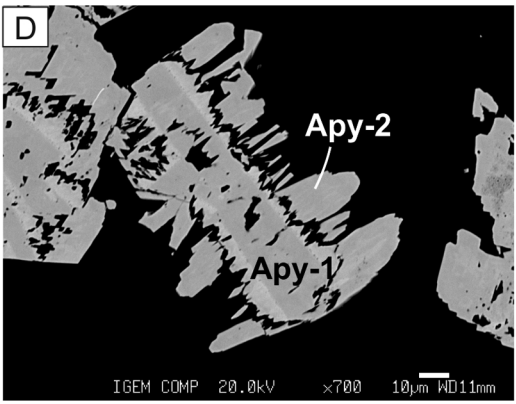

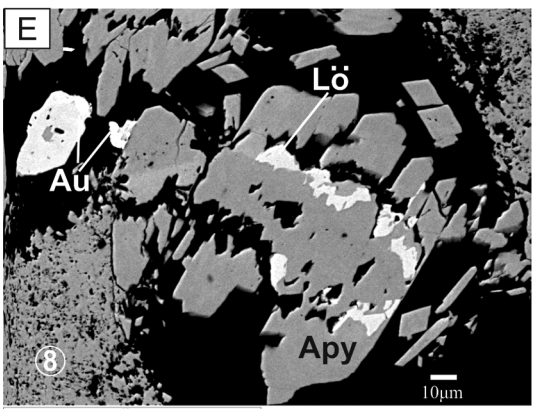

Composition of arsenopyrite, wt. %

№	As	Fe	S	Sb	Co	Total	As/S
1	41.32	36.17	21.31	0.08	0.05	98.97	0.83
2	47.73	34.45	17.13	0.03	0.04	99.4	1.19
3	50.08	33.29	15.25	0.31	0.04	99.02	1.41
4	49.94	33.16	15.27	0.11	0.06	98.54	1.4
5	43.85	36.12	20.17	0.03	0.02	100.23	0.93
6	46.02	34.79	18.14	0.01	0.04	99.02	1.09
7	47.43	34.54	17.46	0	0.05	99.54	1.16
8	46.4	34.08	17.93	0.03	0.03	98.53	1.11

Figure 8

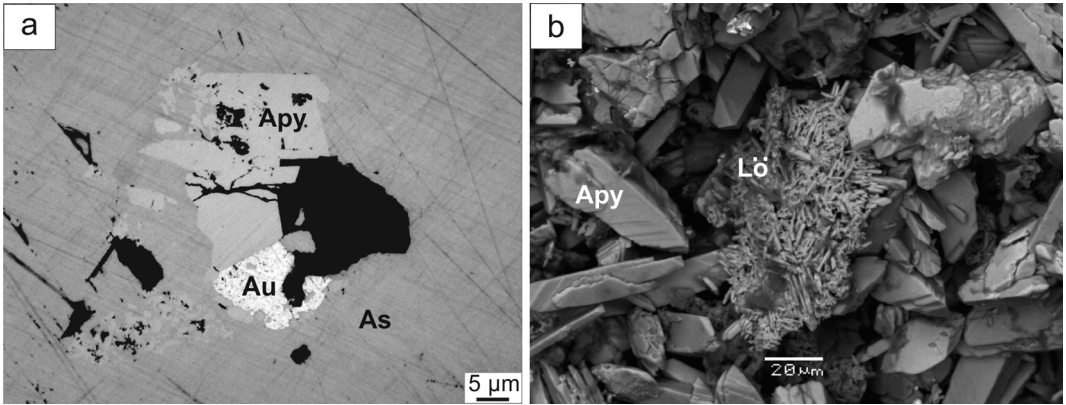

Figure 9

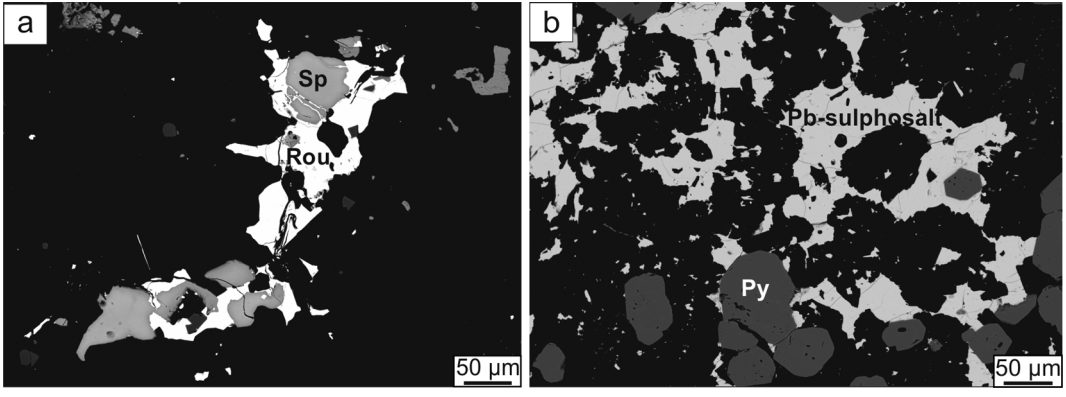

Figure 10

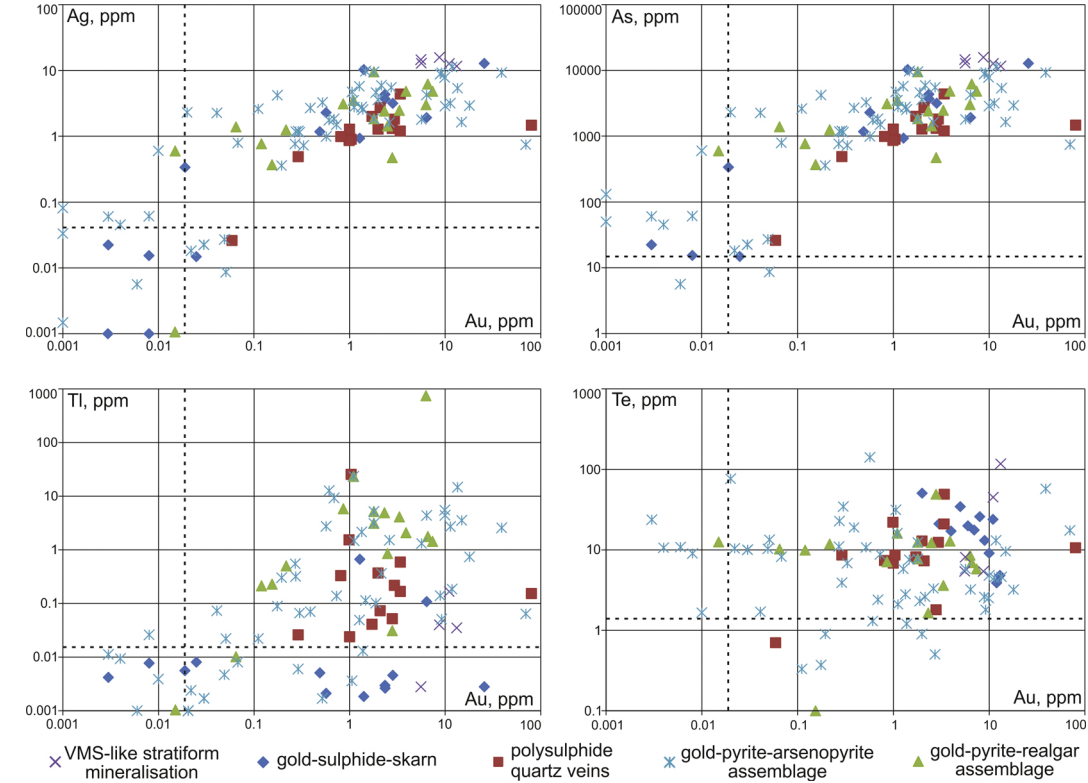
Ag, ppm
Au, ppm
As, ppm
Au, ppm
Tl, ppm
Au, ppm
Te, ppm
Au, ppm
VMS-like stratiform mineralisation
gold-sulphide-skarn
polysulphide quartz veins
gold-pyrite-arsenopyrite assemblage
gold-pyrite-realgar assemblage

Figure 11

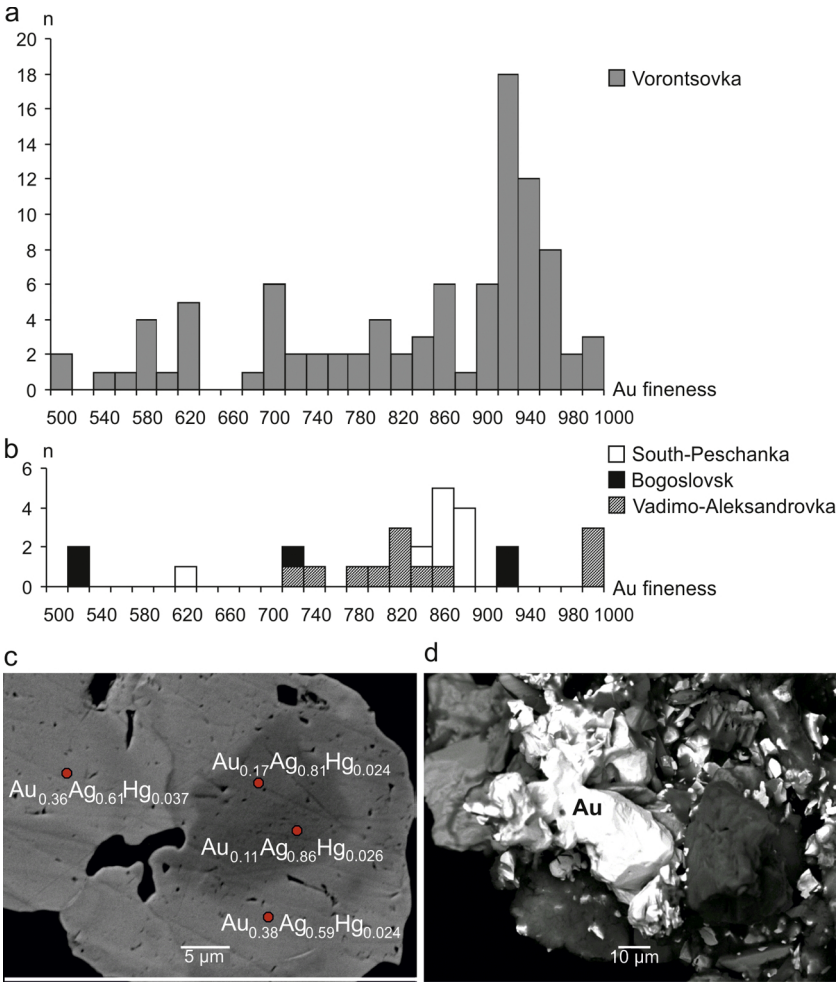
a
n
20
18
16
14
12
10
8
6
4
2
0
Vorontsovka
Au fineness
500 540 580 620 660 700 740 780 820 860 900 940 980 1000
b
n
6
4
2
0
South-Peschanka
Bogoslovsk
Vadimo-Aleksandrovka
Au fineness
500 540 580 620 660 700 740 780 820 860 900 940 980 1000
c
Au0.36Ag0.61Hg0.037
Au0.17Ag0.81Hg0.024
Au0.11Ag0.86Hg0.026
Au0.38Ag0.59Hg0.024
5 μm
d
Au
10 μm

Figure 12

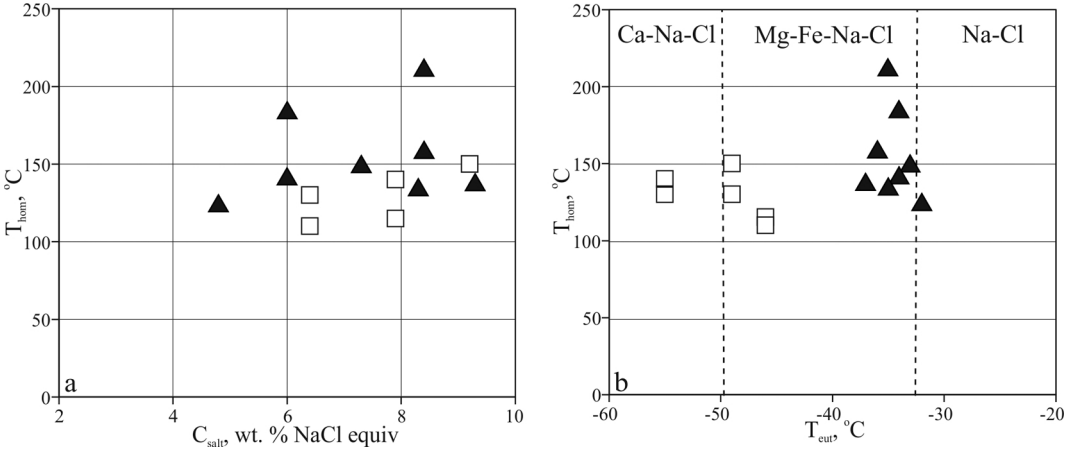
250
200
150
100
50
0
T_{hom}, °C
a
2
4
6
8
10
C_{salt}, wt. % NaCl equiv
Ca-Na-Cl
Mg-Fe-Na-Cl
Na-Cl
b
-60
-50
-40
-30
-20
T_{eut}, °C

Figure 13

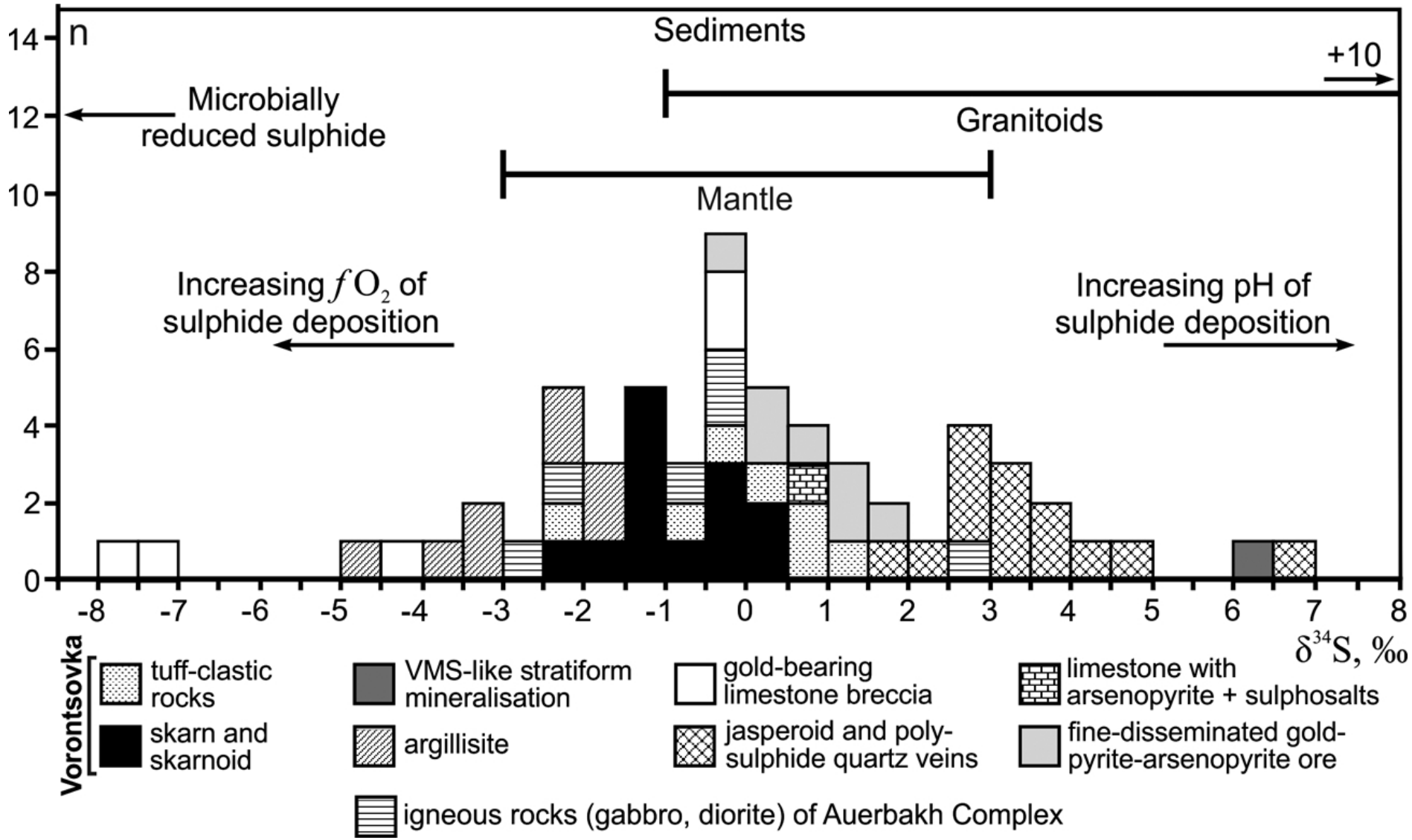
n
Sediments
+10
Microbially reduced sulphide
Granitoids
Mantle
Increasing fO_2 of sulphide deposition
Increasing pH of sulphide deposition
14
12
10
8
6
4
2
0
-8 -7 -6 -5 -4 -3 -2 -1 0 1 2 3 4 5 6 7 8
$\delta^{34}S$, ‰
Vorontsovka
tuff-clastic rocks
skarn and skarnoid
VMS-like stratiform mineralisation
argillisite
gold-bearing limestone breccia
jasperoid and poly-sulphide quartz veins
limestone with arsenopyrite + sulphosalts
fine-disseminated gold-pyrite-arsenopyrite ore
igneous rocks (gabbro, diorite) of Auerbakh Complex

Figure 14

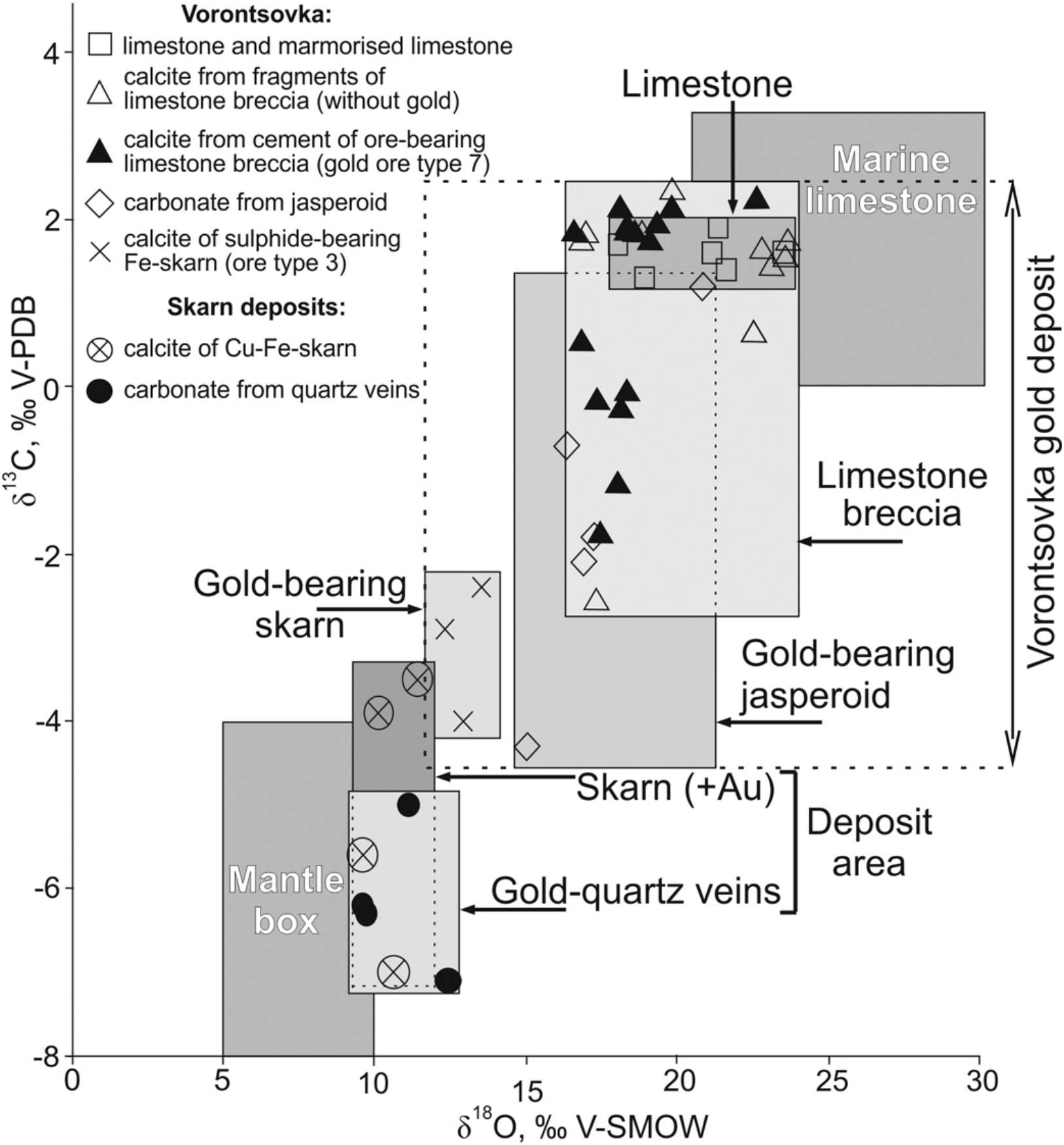
Vorontsovka:
limestone and marmorised limestone
calcite from fragments of limestone breccia (without gold)
calcite from cement of ore-bearing limestone breccia (gold ore type 7)
carbonate from jasperoid
calcite of sulphide-bearing Fe-skarn (ore type 3)
Skarn deposits:
calcite of Cu-Fe-skarn
carbonate from quartz veins
Limestone
Marine limestone
Limestone breccia
Gold-bearing skarn
Gold-bearing jasperoid
Skarn (+Au)
Deposit area
Gold-quartz veins
Mantle box
Vorontsovka gold deposit
δ13C, ‰ V-PDB
δ18O, ‰ V-SMOW
4
2
0
-2
-4
-6
-8
0
5
10
15
20
25
30

Figure 15

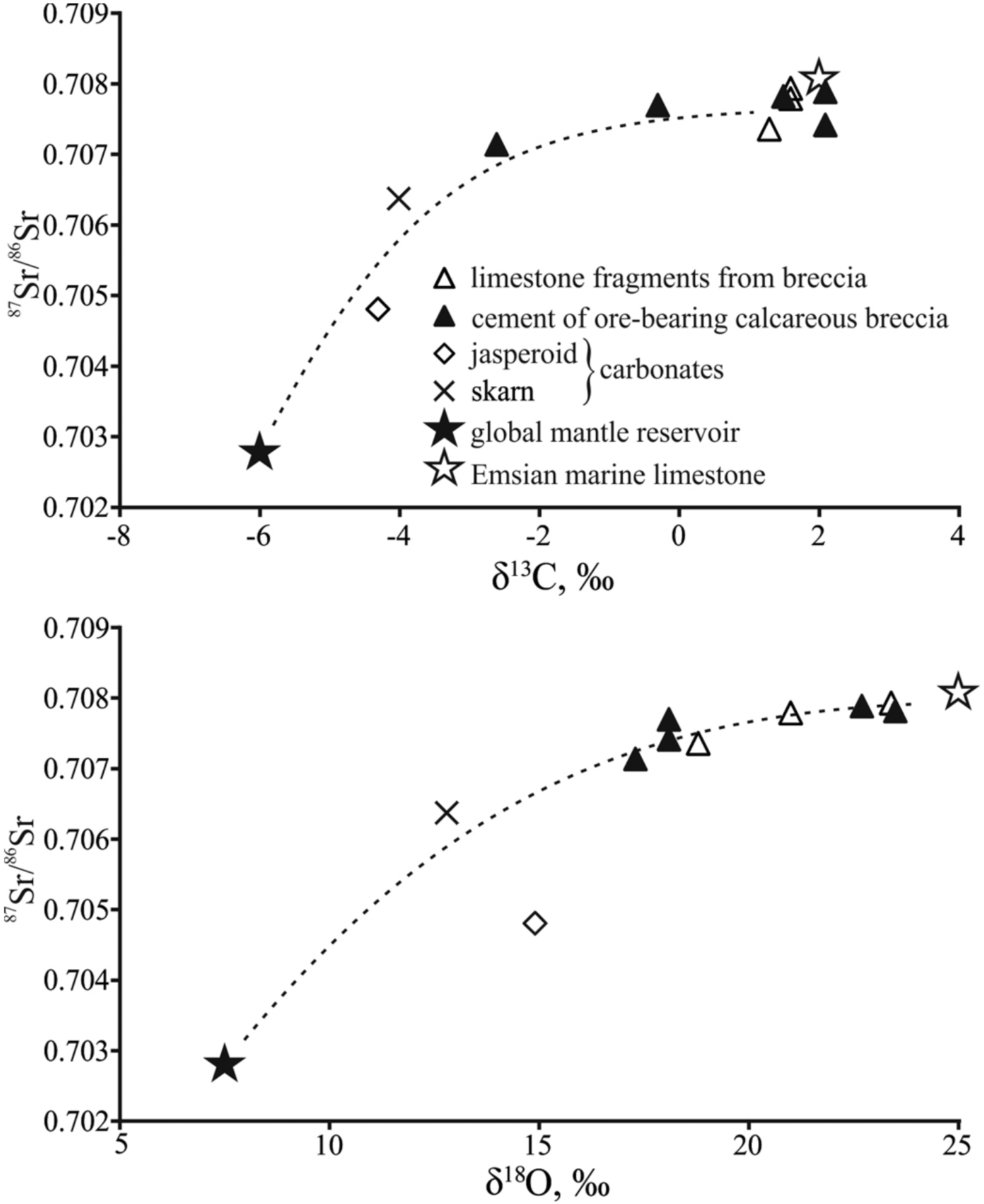
0.709
0.708
0.707
0.706
0.705
0.704
0.703
0.702
$^{87}Sr/^{86}Sr$
-8
-6
-4
-2
0
2
4
$\delta^{13}C$, ‰
limestone fragments from breccia
cement of ore-bearing calcareous breccia
jasperoid
skarn
carbonates
global mantle reservoir
Emsian marine limestone
0.709
0.708
0.707
0.706
0.705
0.704
0.703
0.702
$^{87}Sr/^{86}Sr$
5
10
15
20
25
$\delta^{18}O$, ‰

Figure 16

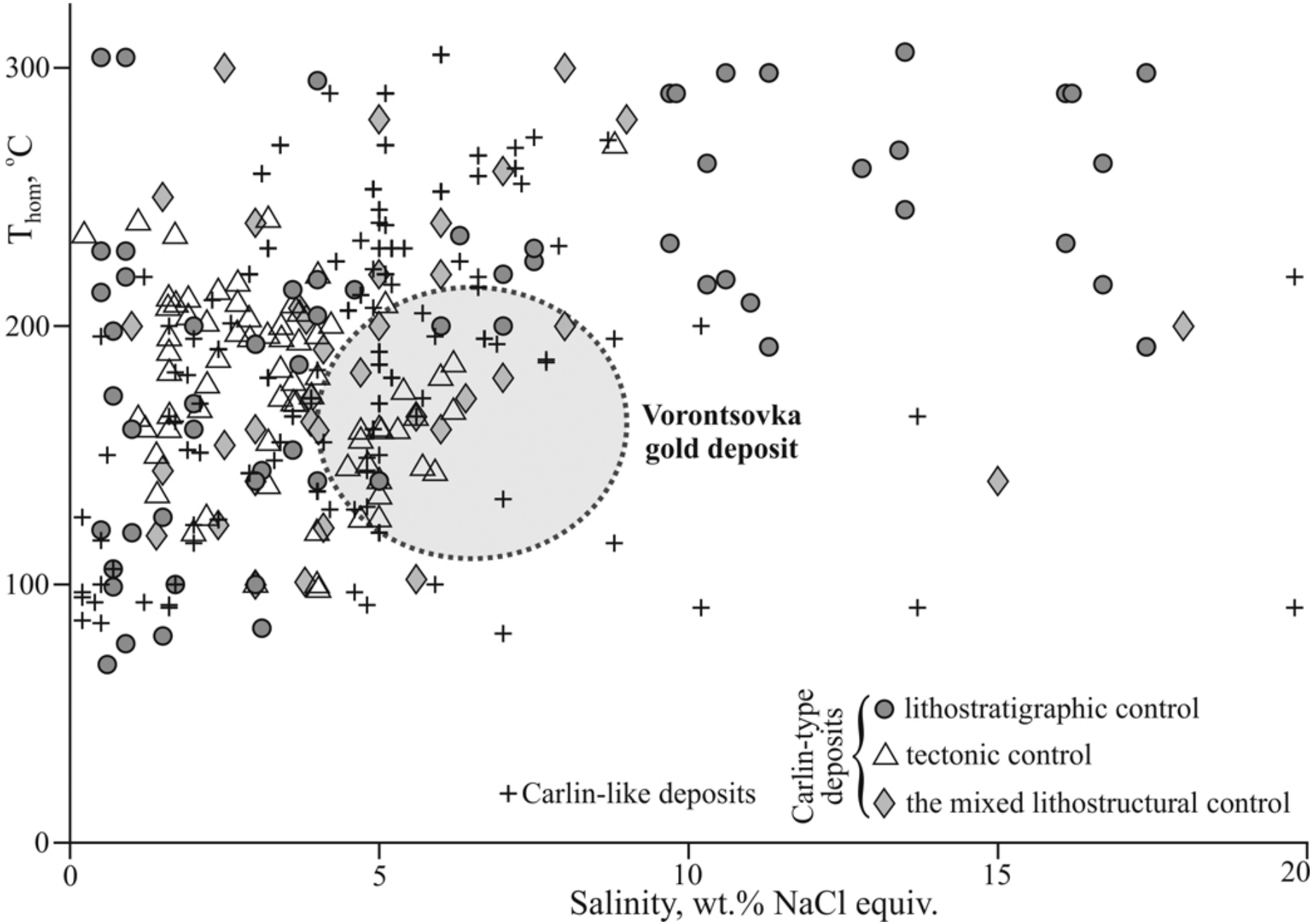
300
200
100
0
T_{hom}, °C
0
5
10
15
20
Salinity, wt.% NaCl equiv.
Vorontsovka
gold deposit
Carlin-like deposits
Carlin-type deposits
lithostratigraphic control
tectonic control
the mixed lithostructural control

Figure 17

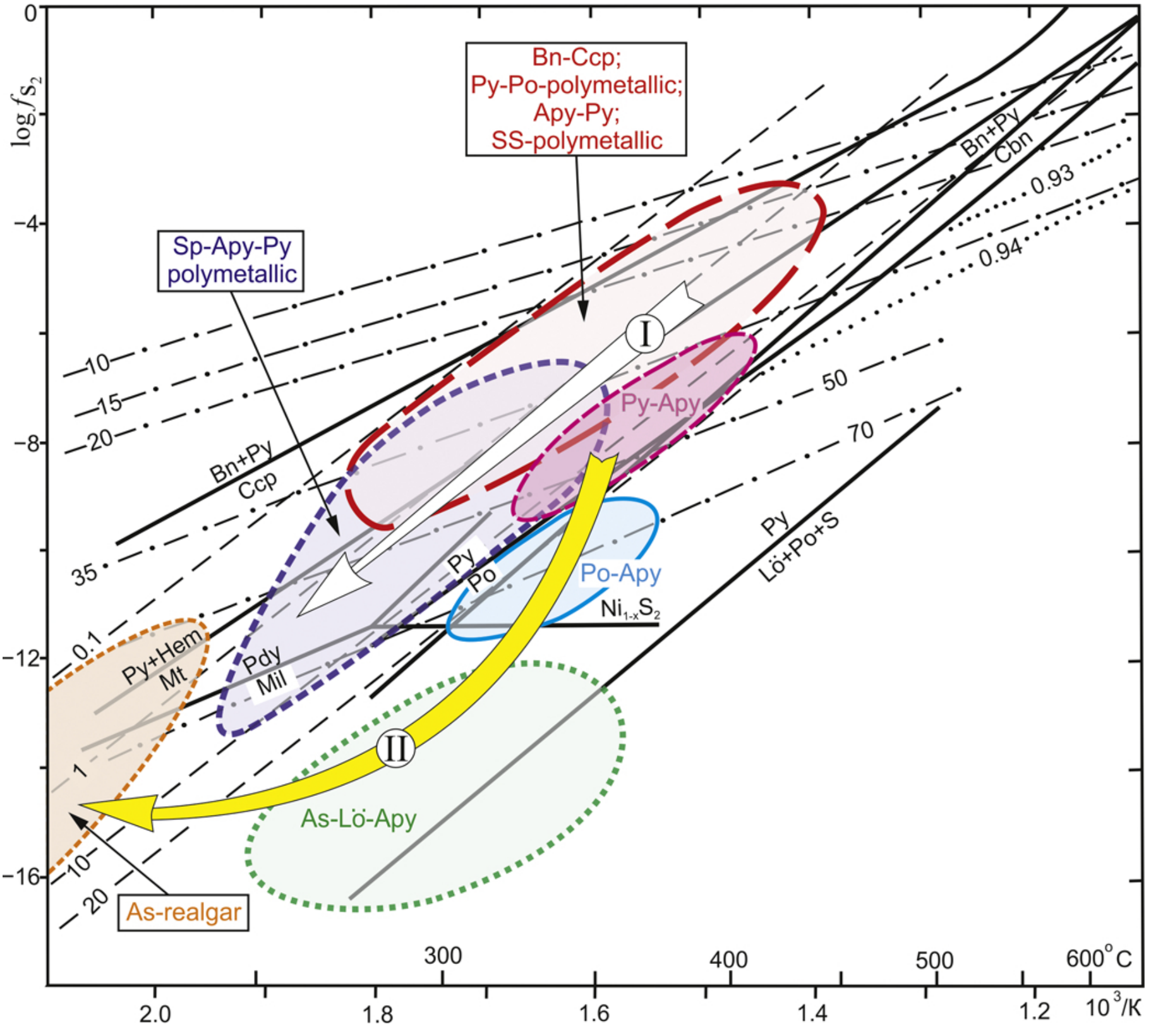
Bn-Ccp;
Py-Po-polymetallic;
Apy-Py;
SS-polymetallic
Sp-Apy-Py
polymetallic
I
II
Py-Apy
Po-Apy
As-Lö-Apy
Bn+Py
Ccp
Bn+Py
Cbn
Py
Po
Ni1-xS2
Py
Lö+Po+S
Py+Hem
Mt
Pdy
Mil
As-realgar
0.93
0.94
10
15
20
35
50
70
0.1
1
10
20
0
−4
−8
−12
−16
log fS2
300
400
500
600° C
2.0
1.8
1.6
1.4
1.2
10 3/K

Figure 18

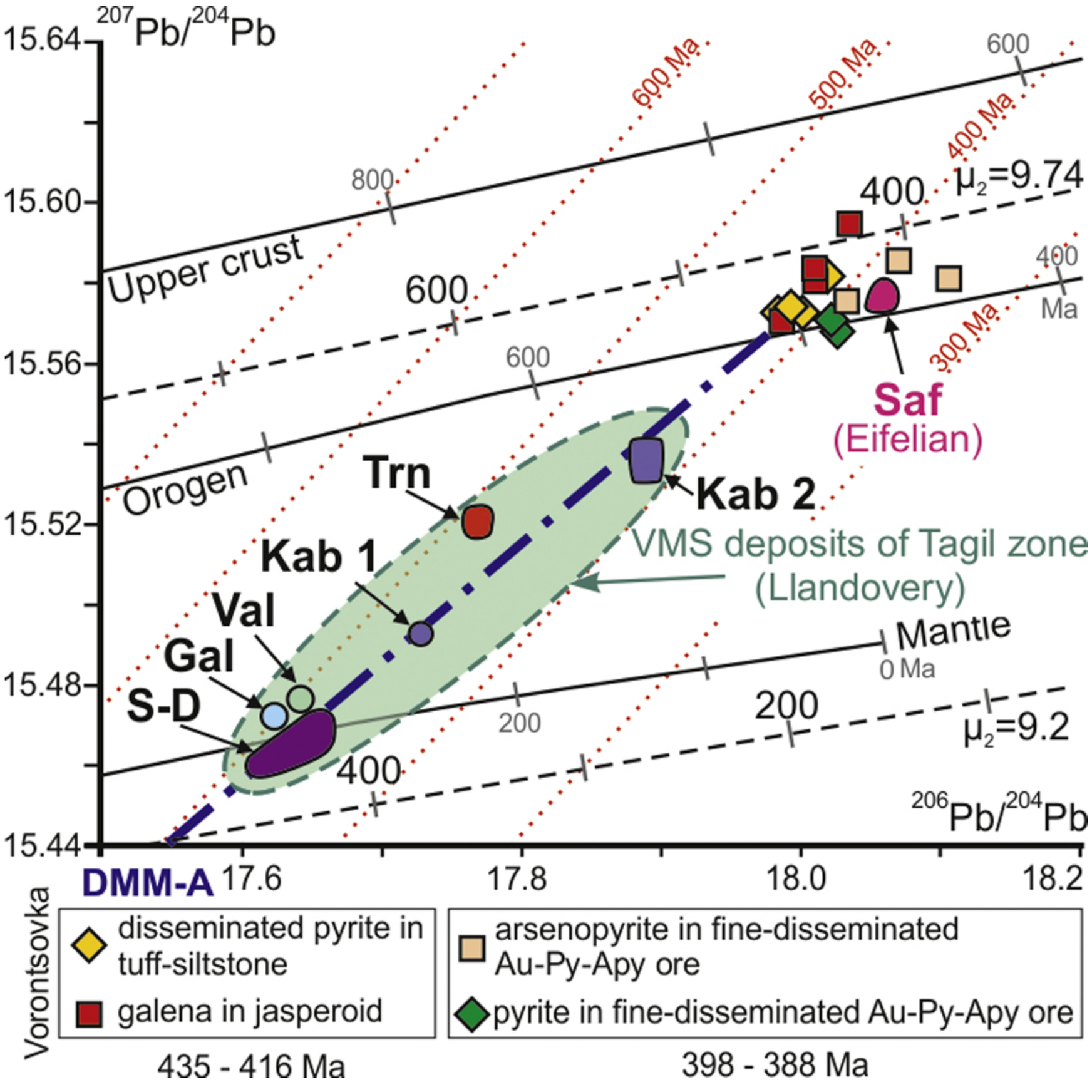
207Pb/204Pb
15.64
15.60
15.56
15.52
15.48
15.44
600 Ma
500 Ma
400 Ma
300 Ma
600
800
400
μ2=9.74
400
Ma
Upper crust
600
600
Orogen
Saf
(Eifelian)
Trn
Kab 2
Kab 1
VMS deposits of Tagil zone
(Llandovery)
Val
Gal
S-D
Mantle
0 Ma
200
200
μ2=9.2
400
206Pb/204Pb
DMM-A
17.6
17.8
18.0
18.2
Vorontsovka
disseminated pyrite in tuff-siltstone
galena in jasperoid
435 - 416 Ma
arsenopyrite in fine-disseminated Au-Py-Apy ore
pyrite in fine-disseminated Au-Py-Apy ore
398 - 388 Ma

Figure 19

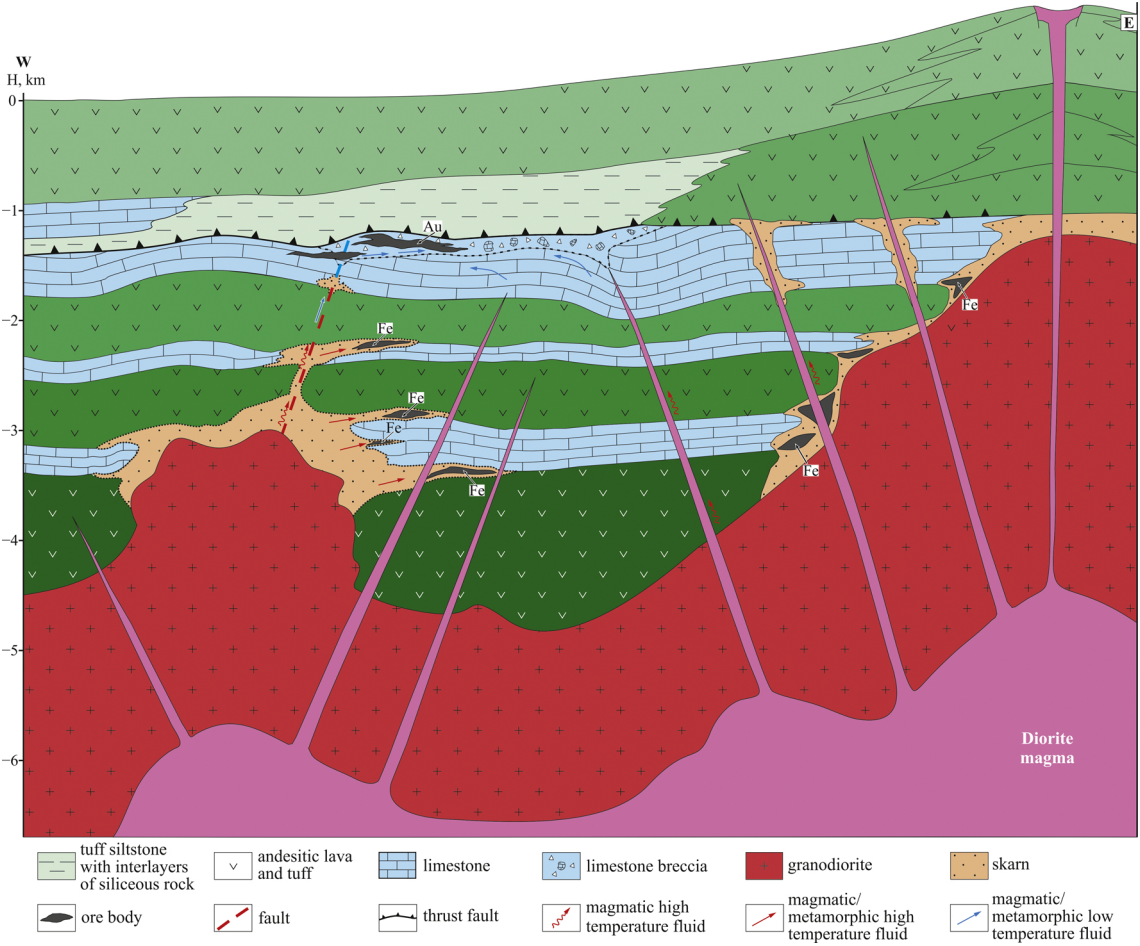
W
H, km
0
−1
−2
−3
−4
−5
−6
E
Au
Fe
Fe
Fe
Fe
Fe
Fe
Diorite
magma
tuff siltstone with interlayers of siliceous rock
andesitic lava and tuff
limestone
limestone breccia
granodiorite
skarn
ore body
fault
thrust fault
magmatic high temperature fluid
magmatic/ metamorphic high temperature fluid
magmatic/ metamorphic low temperature fluid

Figure 20